Ore Geology Reviews 81 (2017) 23–41

Contents lists available at ScienceDirect

Ore Geology Reviews

journal homepage: www.elsevier.com/locate/oregeorev

# REE minerals at the Songwe Hill carbonatite, Malawi: HREE-enrichment in late-stage apatite

Sam Broom-Fendley [a,b,*], Aoife E. Brady [c,1], Frances Wall [a], Gus Gunn [b], William Dawes [c]

[a] Camborne School of Mines, University of Exeter, Penryn Campus, Penryn, Cornwall TR10 9FE, UK
[b] British Geological Survey, Keyworth, Nottinghamshire NG12 5GG, UK
[c] Mkango Resources Ltd., 706 27 Avenue NW, Calgary, Alberta, T2M 2J3, Canada

ARTICLE INFO

*Article history:*
Received 11 March 2016
Received in revised form 23 September 2016
Accepted 19 October 2016
Available online 24 October 2016

*Keywords:*
Apatite
Carbonatite
Rare earth elements
Heavy rare earth elements
Synchysite-(Ce)
Chilwa Alkaline Province
Critical metals
Songwe Hill

ABSTRACT

Compared to all published data from carbonatites and granitoids, the fluorapatite compositions in the Songwe Hill carbonatite, determined by EPMA and LA ICP-MS, have the highest heavy (H)REE concentration of any carbonatite apatite described so far. A combination of this fluorapatite and the REE fluorocarbonates, synchysite-(Ce) and parisite-(Ce), which are the other principal REE bearing minerals at Songwe, gives a REE deposit with a high proportion of Nd and a higher proportion of HREE (Eu–Lu including Y) than most other carbonatites. Since Nd and HREE are currently the most sought REE for commercial applications, the conditions that give rise to this REE profile are particularly important to understand. Multiple apatite crystallisation stages have been differentiated texturally and geochemically at Songwe and fluorapatite is divided into five different types (Ap-0–4). While Ap-0 and Ap-1 are typical of apatite found in fenite and calcite-carbonatite, Ap-2, -3 and -4 are texturally atypical of apatite from carbonatite and are progressively HREE-enriched in later paragenetic stages. Ap-3 and Ap-4 exhibit anhedral, stringer-like textures and their REE distributions display an Y anomaly. These features attest to formation in a hydrothermal environment and fluid inclusion homogenisation temperatures indicate crystallisation occurred between 200–350 °C. Ap-3 crystallisation is succeeded by a light (L)REE mineral assemblage of synchysite-(Ce), strontianite and baryte. Finally, late-stage Ap-4 is associated with minor xenotime-(Y) mineralisation and HREE-enriched fluorite. Fluid inclusions in the fluorite constrain the minimum HREE mineralisation temperature to approximately 160 °C. A model is suggested where sub-solidus, carbonatite-derived, (carbo)-hydrothermal fluids remobilise and fractionate the REE. Chloride or fluoride complexes retain LREE in solution while rapid precipitation of apatite, owing to its low solubility, leads to destabilisation of HREE complexes and substitution into the apatite structure. The LREE are retained in solution, subsequently forming synchysite-(Ce). This model will be applicable to help guide exploration in other carbonatite complexes.



## 1. Introduction

Carbonatites (igneous rocks containing >50% carbonate minerals; Le Maître et al., 2002) are host to some of the largest REE resources (Chakhmouradian and Wall, 2012; Wall, 2014; Verplanck et al., 2016). However the REE-minerals currently extracted from carbonatites (REE-fluorocarbonates, monazite) are typically LREE-rich (La–Sm) and HREE-poor (Eu–Lu + Y; Wall, 2014). With the exception of Nd, they are, therefore, deficient in the majority of the REE considered 'critical', i.e. of high economic importance, but at risk of supply disruption (European Commission, 2014; Gunn, 2014). Only a few examples of carbonatite-related HREE enrichment are known (e.g. Kangankunde, Malawi; Khibiny, Russia; Deadhorse Creek, Canada; Huanglongpu and Huayangchuan, China; Lofdal, Namibia; Pivot Creek, New Zealand; and Bear Lodge, USA; Wall and Mariano, 1996; Zaitsev et al., 1998; Potter and Mitchell, 2005; Xu et al., 2007; Wall et al., 2008; Kynicky et al., 2012; Cooper et al., 2015; Andersen et al., 2016). With the exception of Lofdal, these are typically minor occurrences forming in late-stage fluid-rich environments.

In this study the composition and texture of REE-bearing minerals at the Songwe Hill carbonatite, Malawi, were investigated with the objective of understanding if there is any mineral phase, or stage in the carbonatite evolution, in which HREE enrichment may occur. Particular attention was paid to the relationship between apatite and REE phases because low-tenor HREE enrichment occurs in late-stage apatite at the Tundulu, Kangankunde and Juquiá carbonatites (Ngwenya, 1994; Wall and Mariano, 1996; Broom-Fendley et al., 2016a; Walter et al., 1995).

*Abbreviations:* L, liquid; V, vapour; TREO, total rare earth oxides.

* Corresponding author at: Camborne School of Mines, University of Exeter, Penryn Campus, Penryn, Cornwall TR10 9FE, UK.
*E-mail address:* s.l.broom-fendley@ex.ac.uk (S. Broom-Fendley).
[1] Present address: IGS (International Geoscience Services) Ltd., Geoscience Innovation Hub, British Geological Survey, Environmental Science Centre, Keyworth, Nottingham NG12 5GG, UK.

http://dx.doi.org/10.1016/j.oregeorev.2016.10.019

Furthermore, the REE have been identified as a potential co- or by-product of phosphate production (Mariano and Mariano, 2012; Ihlen et al., 2014).

Fluorapatite ($Ca_5(PO_4)_3F$), is ubiquitous in carbonatites and is typically a liquidus phase, but can occur through early magmatic to late hydrothermal stages (Eby, 1975; Kapustin, 1980; Hogarth, 1989). It readily accommodates the REE in its structure (Pan and Fleet, 2002; Hughes and Rakovan, 2015). Consequently, the timing of apatite crystallisation during carbonatite evolution can strongly affect the whole-rock REE distribution of a carbonatite and the likelihood of REE deposit formation (Zaitsev et al. 2015). Apatite habits can vary with the conditions of formation (e.g. Wyllie et al., 1962), and compositional variation in apatite has been demonstrated to track the magmatic and hydrothermal evolution of alkaline rocks (Zirner et al., 2015; Ladenburger et al., 2016). Similarly, apatite can elucidate the relationship between carbonatites and associated alkaline rocks (Le Bas and Handley, 1979; Stoppa and Liu, 1995; Wang et al., 2014), trace carbonatite evolution (Walter et al., 1995), and provide information on the process of REE mineralisation (Campbell and Henderson, 1997; Broom-Fendley et al., 2016a).

Considering the above characteristics, a secondary objective of this study is to elucidate the composition of late-stage carbonatite-derived fluids and understand mechanisms for REE transport and fractionation. To this end, trace element analyses of apatite, fluorite and other REE-bearing minerals, are presented, as well as a preliminary fluid-inclusion study.

## 2. The Songwe Hill carbonatite

The Songwe Hill carbonatite is located in south-eastern Malawi, near the Mozambique border, and is part of the Chilwa Alkaline Province (Fig. 1). This province is an essentially intrusive suite of Early Cretaceous alkaline rocks intruded into Precambrian basement (Garson, 1965; Woolley, 2001). Songwe is the fourth largest of the carbonatites in the province and exploration work by Mkango Resources Ltd. has established a (NI 43-101 compliant) mineral resource estimate, comprising an indicated and inferred component of 13.2 million tonnes (grading 1.62% Total Rare Earth Oxide (TREO)) and 18.6 million tonnes (grading 1.38% TREO) respectively, using a cut-off grade of 1% TREO (Croll et al., 2014).

The geology of the Songwe Hill carbonatite is described in detail in Croll et al. (2014) and Broom-Fendley (2015) and only a brief overview is presented here. There is evidence for a coarse-grained calcite carbonatite (C1) at depth; however, most exposed rocks at Songwe comprise two, fine-grained, carbonatites (Fig. 1C), which incorporate varying proportions of brecciated fenite. The earlier stage is a light grey, calcite carbonatite (C2) and the latter is darker and more Fe-rich, termed ferroan calcite carbonatite (C3). REE concentrations are higher in the later-stages of the intrusion, with total REE concentrations in C2 and C3 carbonatite averaging approximately 15,000 and 30,000 ppm, respectively (Broom-Fendley, 2015). The carbonatite is cross-cut by numerous, laterally discontinuous, late-stage veins varying in width between 1 cm and approximately 1 m. These veins include REE-rich apatite-fluorite veins and, lastly, Fe-Mn-veins caused by low temperature alteration. The intrusion is surrounded by a fenitized and commonly brecciated aureole, extending for an unknown distance from the intrusion.

## 3. Methodology

Samples were obtained from diamond drill-core drilled by Mkango Resources in 2011 and 2012. Specimens with high whole-rock $P_2O_5$ concentrations were selected to ensure the presence of apatite. Petrography was carried out using cold-cathodoluminescence (CL) and SEM (using the same techniques as described in Broom-Fendley et al., 2016a) before samples were analysed for trace elements using electron probe micro-analyser (EPMA) and laser ablation inductively coupled plasma mass spectrometry (LA-ICP-MS).

EPMA analyses were undertaken at the British Geological Survey (BGS) and Natural History Museum (NHM), London, using a FEI-Quanta 600 scanning electron microscope (SEM) and Cameca SX100 electron microprobe, respectively. The BGS-SEM was operated using the same method detailed in Walters et al. (2013) and Broom-Fendley et al. (2016a). The operating conditions for the NHM EPMA were 20 kV and 20 nA with a beam size of 5–10 μm. Peak counting times were 20 s for Na, Ca, Mn, P, La, Ce, Cl; 30 s for F, Si, Fe, Pr, Nd, Gd, S; 40 s for Sm, Dy, and 60 s for Y when analysing for apatite and 20 s for Na, Mg, Al, Ca, Mn, P, La, Ce, Cl; 30 s for F, Si, Fe, Pr, Nd, Eu, Gd, S; 40 s for Sm, Dy; 60 s for Y; and 120 s for Th when analysing for REE minerals. Background-counting times were half the peak value. X-ray counts were converted to wt% oxide using the Cameca PAP correction program. Empirical interference corrections were performed for La, Ce and the HREE following Williams (1996). Correction factors were calculated by measuring the interferences observed on individual REE reference standards. A variety of natural and synthetic primary reference materials were used with an internal apatite standard for quality control.

Trace elements were analysed, using LA ICP-MS, at the BGS and at Aberystwyth University in Wales. Ablation at the BGS utilized the same methodology as described in Broom-Fendley et al. (2016a). The laser system at Aberystwyth is based on a Coherent/Lambda Physik Compex Pro excimer ArF laser, working at 193 nm, coupled to a Coherent/Lambda Physik GeoLas Pro ablation system. The spot size was 20 μm with a repetition rate of 5 Hz and a corresponding fluence of 10 J $cm^{-2}$. Ablated material was analysed using a Thermo-Finnigan Element 2 high resolution ICP-MS, obtaining 10 spectra over 24 s. Analyses were calibrated using SRM 610 as an external standard and SRM 612 as a check standard.

Microthermometric analyses were carried out at the BGS and at McGill University, Canada, using a Linkam THM600 and a TS1500 stage, respectively. Instrument calibration utilized synthetic fluid inclusion standards at −56.6, 0 and 374 °C. Estimated analytical error is ±0.2 °C for low (<50 °C) and ±2 °C for higher (>75 °C) temperatures.

## 4. Paragenesis of apatite and other REE-bearing minerals

REE minerals at Songwe Hill include REE-fluorocarbonates, florencite-(Ce), and minor xenotime-(Y). Importantly, the REE also occur as minor and trace elements in fluorapatite, calcite and fluorite. Compositional data and textural observations for apatite, synchysite-(Ce), florencite-(Ce), fluorite and xenotime-(Y) are presented in paragenetic order in the following subsections, with the interpreted paragenetic sequence summarised in Fig. 2. The composition and texture of apatite is highly variable and is divided into five groups (Ap-0–4; Table 1).

### 4.1. Ap-0 (fenite)

Ap-0 occurs in potassic fenite, outside of the main Songwe carbonatite. It is characterised by large (typically >0.1 mm), partially fragmented anhedral grains, in association with altered K-feldspar and minor zircon. Under CL Ap-0 luminesces purple–mauve, and is compositionally homogeneous in BSE images (Table 1).

All apatite at Songwe is fluorapatite. Ap-0 has the highest $SiO_2$ and $SO_3$ concentration of all the analysed apatite types, but lower U, Th and Na (Tables 2 and 3; Fig. 3). It is strongly enriched in the LREE with a near-linear REE distribution decreasing towards the HREE, and a small negative Eu-anomaly (Fig. 4).

### 4.2. Ap-1, Ap-2, (C1—early igneous carbonatite)

Ovoid apatite occurs in early (C1) calcite carbonatite and is subdivided into Ap-1 and Ap-2, respectively representing cores and

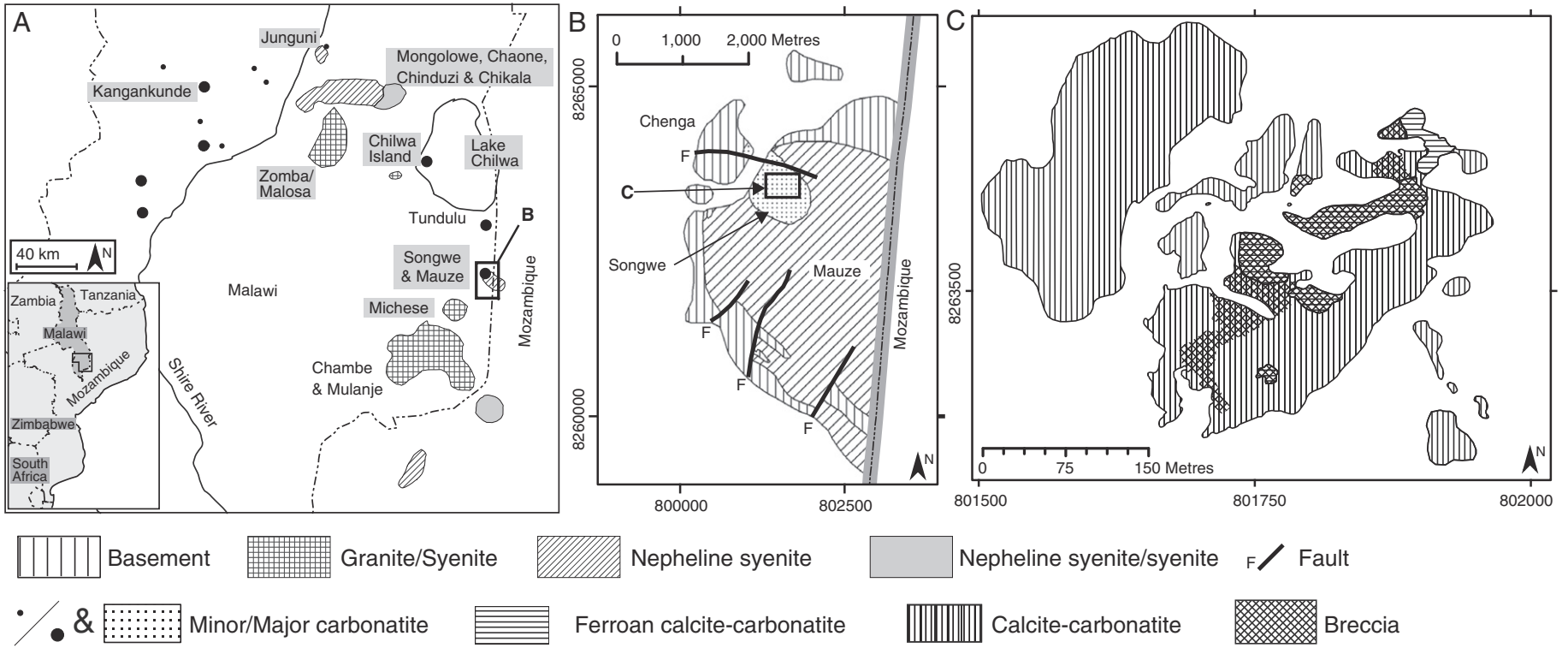


**Fig. 1.** Simplified geological maps showing the location of Songwe in the Chilwa Alkaline Province (A), Mauze (B) and the Songwe Hill carbonatite (C). Coordinates: UTM 36S Grid; WGS 1984 datum. Redrawn after Woolley (2001), Garson (1965), Croll et al. (2014) and Broom-Fendley (2015).

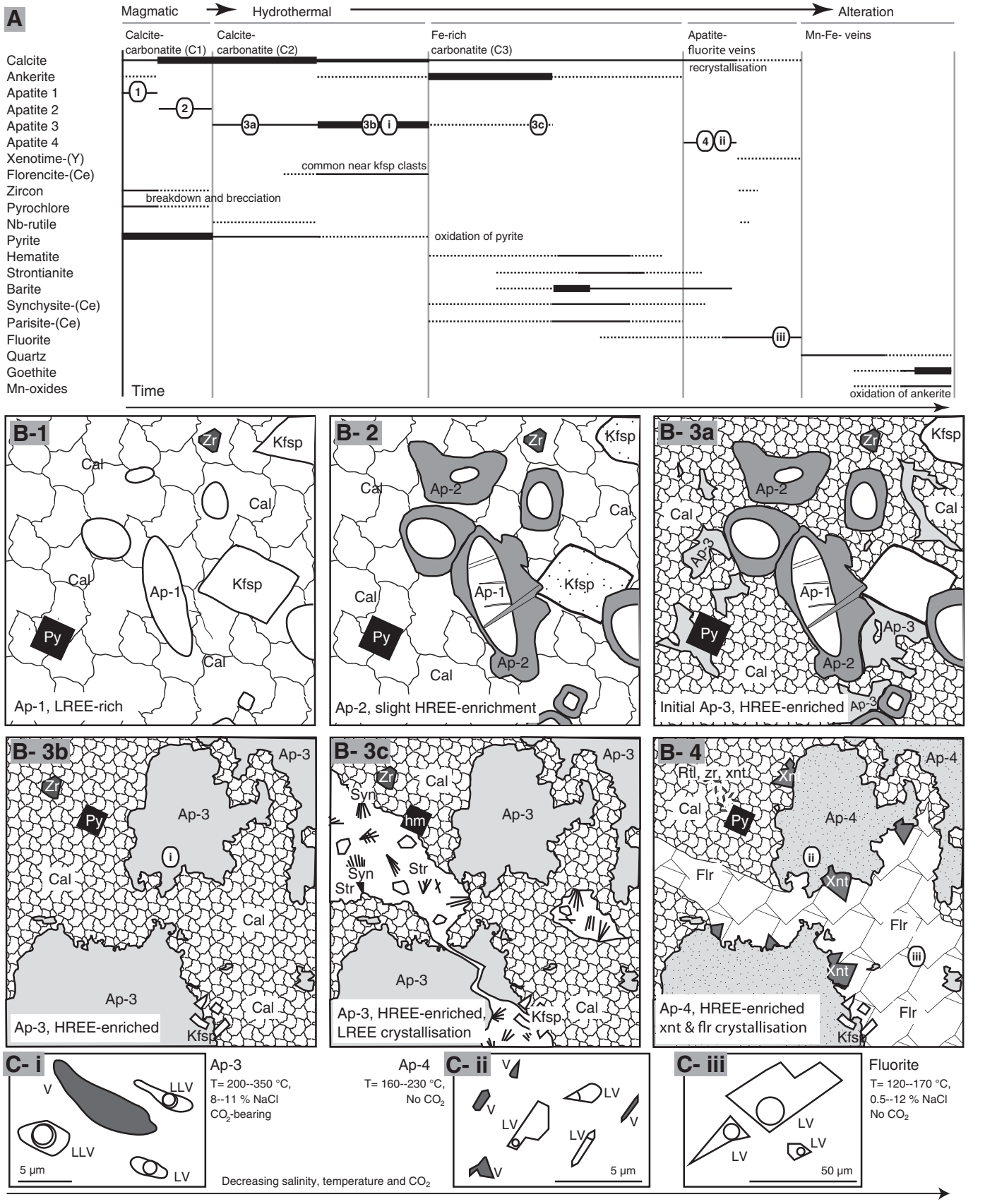


**Fig. 2.** Summary paragenetic (A) and schematic diagrams of the different stages of REE mineralisation (B) and fluid inclusion habits (C) at Songwe Hill. Arabic numerals in (A) correspond to separate panels in (B) while roman numerals correspond to diagrams in (C). Abbreviations: Cal, calcite; py, pyrite; zr, zircon; Kfsp, K feldspar; syn, synchysite-(Ce) str, strontianite; hm, hematite; rtl, rutile; xnt, xenotime-(Y); flr, fluorite; L, liquid; V, vapour. See Table 1 for apatite types.

**Table 1**
Summary of the textural differences between the different apatite types.

| Apatite type | Rock types present | Texture | CL colour* | BSE features |
|---|---|---|---|---|
| Ap-0 | Fenite | Anhedral, fragmented | Purple/mauve | Featureless |
| Ap-1 | Calcite-carbonatite (C1) | Ovoid - cores | Purple | Zoning, spongey and fractured |
| Ap-2 | Calcite-carbonatite (C1) | Ovoid - rims | Blue/green | Zoned and fractured |
| Ap-3 | Calcite-carbonatite (C2) and ferroan calcite-carbonatite (C3) | Anhedral, veins and stringers | White/purple | Spongey, darker ovoid patches |
| Ap-4 | Apatite-fluorite veins | Anhedral, locally euhedral overgrowths | Purple/green | Spongey with xenotime overgrowths |

Note: *Selected CL spectra are available in Supplementary Fig. 1.

rims. These two apatite types are differentiable in CL and BSE images: Ap-1 is violet while Ap-2 is light blue under CL, and brighter in BSE images (Fig. 5). Ovoid apatite is associated with large (>100 μm) euhedral to subhedral calcite, euhedral to subhedral zircon, minor pyrochlore and fragmented laths of K-feldspar.

Ap-1 and Ap-2 are compositionally similar; REE contents positively correlate with Na, although the correlation is tighter for Y than Ce (Fig. 3A–D). Ap-1 typically has the lowest REE, Na, U and Th concentrations and moderate Sr concentration relative to the other apatite types (Fig. 3). Ap-1 has a REE distribution similar to Ap-0, but with a lower LREE concentration, no Eu anomaly and a negative Y anomaly (Fig. 4). Ap-2 has higher Sr and Ce, slightly higher $SiO_2$ and slightly lower $Na_2O$ concentrations relative to Ap-1. Ap-2 has the same LREE distribution as Ap-1, but exhibits elevated HREE-contents around Dy.

Ap-1 is compositionally and texturally similar to 'typical' early apatite in carbonatites, in that it forms bands of LREE-rich ovoid grains, reflecting crystallisation from a turbulent LREE-rich melt (Le Bas, 1989; Hornig-Kjarsgaard, 1998; Bühn et al., 2001; Zaitsev et al., 2015). These characteristics provide reasonable evidence that Ap-1 is one of the earliest apatite generations to crystallise at Songwe (Fig. 2).

Evidence for a change in crystallisation conditions is present in the overgrowth of Ap-1 by Ap-2, the latter being more HREE enriched (Fig. 4). Post-ablation assessment of LA spots using a SEM indicated that the HREE-enriched data are not due to contamination from another phase. It is, therefore, likely that the Ap-2 rims represent a shift towards a more HREE-enriched crystallisation environment. Neither overgrowths nor continued crystallisation occur in zircon or pyrochlore, associated with Ap-1, and these are considered to be a product of early formation only (Fig. 2).

### 4.3. Ap-3 (C2, C3—main Songwe carbonatite)

Ap-3 is the most abundant apatite type at Songwe. It occurs as an anhedral groundmass and as stringers in calcite carbonatite (C2), late-stage ferroan calcite carbonatite (C3) and in Mn-Fe-veins (Fig. 6). In one example (T0206) Ap-3 occurs as an overgrowth on Ap-1/Ap-2 grains, illustrative of the crystallisation sequence of these minerals (Fig. 5B). A wide range of mineral phases are associated with Ap-3, including fluorite, sulphides (predominantly pyrite, but also rare sphalerite and galena), anhedral calcite, ankerite and fragmented K-feldspar. Ap-3 is texturally complex, but has a similar habit and complexity in all of the carbonatite types. Under CL it commonly luminesces bright white–purple (Fig. 6A–B), with emission bands at approximately 475, 540, 575, 600 and 650 nm, corresponding to $Dy^{3+}$, $Sm^{3+}$ and $Tb^{3+}$ (see Supplementary Fig. 1). This emission spectra corresponds to 'group 1', apatites (after Mitchell, 2014), where $Ce^{3+}$, $Eu^{2+}$ and $Eu^{3+}$ lines, commonly attributed to blue CL luminesce, are absent. Some areas of Ap-3 luminesce darker purple or greenish-yellow, most-likely related to small changes in apatite composition.

Ap-3 has higher Na and REE concentrations than Ap-1 and -2 and more variable Sr contents (Fig. 3). The positive correlation between Na and the REE in Ap-1 and Ap-2 is also present in Ap-3 (Fig. 3A). This trend is strongest between Na and the HREE, especially in calcite carbonatite. Ap-3 has higher concentrations of U and Th than Ap-1 and Ap-2, with a high-Th trend and a lower-Th, higher-U trend (Fig. 3E–F). Increasing concentration of U and Th corresponds with increasing HREE contents, although there is considerable sample variability. Ap-3 from Mn-Fe-veins displays a significantly different trend to apatite from other carbonatite types as the REE negatively correlate with Sr (Fig. 3G).

The REE distributions of Ap-3 are HREE enriched relative to other apatite compositions from carbonatites (e.g. Hornig-Kjarsgaard, 1998), and are all HREE-enriched, relative to Ap-1 and -2 (Fig. 4). For clarity, they are sub-divided into four groups: (1) flat REE distribution, with less HREE than LREE; (2) slightly convex-up distribution, with similar chondrite-normalised concentrations of the HREE and LREE, and a negative Y anomaly; (3) convex-up distribution, centred on Gd, with a small negative Y anomaly; and (4) LREE-poor, with a strong Dy enrichment and small negative Y anomaly (Fig. 4C–F, respectively). No common pattern is evident between the distributions of apatite from the different carbonatite types.

Rare irregular clusters of fluid inclusions occur in Ap-3. These commonly appear disrupted and opened (Fig. 7A). They are interpreted as primary inclusions as they are randomly distributed away from grain boundaries. Fluid inclusion assemblages from Ap-3 comprise single vapour-phase (V) inclusions, mixed 2-phase aqueous liquid-vapour (LV) and three-phase carbonic liquid and vapour (LLV) with 5–40% vapour bubble volume (estimated using techniques after Shepherd et al., 1985). Trapped solids are also present in a small number of inclusions: these are rusty brown under PPL and isotropic under XPL indicating that they are probably Fe-oxides.

Microthermometric data were collected from 38 inclusions (Supplementary data), comprising a mixture of three-phase LLV and two-phase LV inclusions. In the LLV inclusions, the carbonic phase melts at −56.75 °C (median) indicating that the inclusions are relatively pure $CO_2$. Clathrate melting occurs between 1.8–6.9 °C (median 4.9 °C) corresponding to a salinity range of 8–11 wt% NaCl equivalent (Diamond, 1992). $CO_2$ homogenisation to liquid (LH) occurs between 13.4–29.9 °C (median 27.65 °C). Homogenisation to a single liquid phase occurred between 200–350 °C (median 290 °C) if an outlier LV inclusion is excluded (Fig. 8). These temperatures are likely to be close to the temperature of the fluid during crystallisation as the intrusions were emplaced at approximately 3 km depth (Eby et al., 1995), equivalent to 90 MPa lithostatic, or 30 MPa hydrostatic pressure. Such low pressures have little effect on the difference between homogenisation temperatures and the true fluid temperature (Bodnar, 2003).

Ap-3 occurs relatively late in the paragenetic sequence as it cross-cuts C2 and C3 carbonatites (Fig. 2). It also occurs in brecciated rocks, forming around fenite and carbonatite fragments. The habit of this apatite type, forming schlieren, patches and microvienlets, is similar to late-stage apatite from other localities (e.g. Kapustin, 1980; Ting et al., 1994). Carbonatites commonly show evidence of multiple stages of fluid reworking, with apatite known to crystallise until relatively late stages of carbonatite emplacement (Kapustin, 1980; Hogarth, 1989; Ting et al., 1994; Broom-Fendley et al., 2016a). These late-stage apatite types are generally associated with one or more generations of carbo-hydrothermal fluids. The presence of fluid inclusions and an Y/Ho anomaly (Fig. 4) also attest to a late hydrothermal environment. In hydrothermal fluids, complexes of $YF_2^+$ are more stable than the equivalent complexes with Dy or Ho (Bau, 1996; Loges et al., 2013), leading to fractionation between Y and Ho where precipitation is controlled by the stability of the REE in solution.

**Table 2**
Representative apatite compositions obtained by EMPA.

| | Fenite | Calcite carbonatite (C1) | | | | Calcite carbonatite (C2) | | | | | | | | Ferroan calcite carbonatite (C3) | | | Ap-Fl-veins | | | Mn-Fe veins | |
|---|---|---|---|---|---|---|---|---|---|---|---|---|---|---|---|---|---|---|---|---|---|
| | Ap-0 | Ap-1 | | Ap-2 | | Ap-3 | | | | | | | | Ap-3 | | | Ap-4 | | | Ap-3 | |
| | T0134 | T0206 | T0218 | T0206 | T0218 | T0327* | T0322* | T0322* | T0324* | T0324* | T0262 | T0225 | T0206 | T0250 | T0167 | U4904 | T0134 | T0178C | U4909 | U4927 | T0227 |
| *Representative analyses* | | | | | | | | | | | | | | | | | | | | | |
| $Na_2O$ | 0.15 | 0.96 | 0.23 | 0.11 | 0.77 | 0.63 | 0.56 | 0.47 | 0.46 | 0.47 | 0.23 | 0.42 | 1.23 | 0.74 | 0.34 | 0.61 | 0.49 | 0.84 | 1.20 | 0.73 | 0.69 |
| $SiO_2$ | 0.90 | – | 0.06 | – | – | 0.01 | – | 0.01 | – | – | – | – | – | – | – | – | – | – | – | – | – |
| $P_2O_5$ | 41.68 | 41.25 | 42.78 | 43.63 | 42.37 | 40.56 | 41.30 | 40.97 | 40.55 | 39.79 | 40.29 | 42.23 | 41.09 | 42.44 | 40.72 | 42.19 | 41.18 | 41.29 | 41.29 | 42.35 | 42.42 |
| CaO | 53.53 | 50.02 | 52.93 | 54.26 | 51.52 | 52.58 | 53.54 | 53.70 | 54.02 | 54.12 | 52.13 | 52.72 | 49.17 | 52.01 | 53.72 | 51.94 | 54.11 | 53.17 | 49.70 | 51.76 | 51.97 |
| MnO | – | – | – | – | – | – | – | – | 0.19 | 0.06 | – | – | – | – | – | – | – | – | – | – | – |
| FeO | 0.10 | – | – | – | – | – | – | 0.04 | 0.13 | 0.28 | 1.39 | – | – | – | – | 0.15 | – | 0.12 | – | – | – |
| SrO | 0.61 | 2.19 | 2.05 | 2.35 | 2.76 | 1.69 | 1.57 | 1.42 | 1.40 | 1.24 | 1.60 | 2.54 | 2.66 | 1.32 | 1.79 | 1.84 | 2.02 | 1.25 | 3.05 | 1.38 | 1.62 |
| $Y_2O_3$ | 0.10 | 1.60 | – | – | 0.77 | 0.54 | 1.07 | 0.85 | 0.99 | 0.84 | 0.15 | – | 3.62 | 1.19 | – | – | – | 0.38 | 1.07 | 0.66 | 0.85 |
| $La_2O_3$ | 0.36 | – | – | – | – | 0.12 | 0.05 | – | – | – | – | – | – | – | – | – | – | – | – | – | – |
| $Ce_2O_3$ | 0.93 | 0.40 | – | – | – | 0.34 | 0.19 | 0.15 | 0.06 | 0.10 | – | – | – | 0.21 | – | 0.50 | – | – | 0.37 | 1.23 | 0.66 |
| $Pr_2O_3$ | | | | | | 0.06 | 0.02 | 0.03 | 0.08 | 0.01 | | | | | | | | | | | |
| $Nd_2O_3$ | | | | | | 0.37 | 0.23 | 0.22 | 0.11 | 0.13 | | | | | | | | | | | |
| $Sm_2O_3$ | | | | | | 0.03 | 0.05 | – | – | – | | | | | | | | | | | |
| $Gd_2O_3$ | | | | | | 0.16 | 0.19 | 0.17 | 0.15 | 0.11 | | | | | | | | | | | |
| $Dy_2O_3$ | | | | | | 0.10 | 0.20 | 0.16 | 0.14 | 0.14 | | | | | | | | | | | |
| $SO_3$ | 0.32 | – | 0.12 | – | 0.25 | 0.25 | 0.04 | – | 0.04 | 0.04 | – | – | 0.15 | – | – | 0.15 | – | 0.25 | 0.55 | – | – |
| F | 5.60 | 6.17 | 5.82 | 5.78 | 5.85 | 5.06 | 4.60 | 5.00 | 4.74 | 5.00 | 5.81 | 5.04 | 5.92 | 5.64 | 2.69 | 4.66 | 3.14 | 5.41 | 5.59 | 4.98 | 4.79 |
| Cl | – | – | – | – | – | 0.01 | – | 0.01 | – | – | – | – | – | – | – | – | – | – | – | – | – |
| Sub-total | 103.41 | 102.58 | 104.00 | 106.13 | 104.29 | 102.52 | 103.57 | 103.00 | 103.06 | 102.33 | 101.60 | 102.96 | 103.83 | 103.56 | 99.06 | 102.05 | 100.66 | 102.71 | 102.83 | 103.09 | 103.09 |
| $O \equiv F_2$, $Cl_2$ | 1.98 | 2.60 | 2.45 | 2.43 | 2.46 | 2.13 | 1.94 | 2.02 | 2.00 | 2.10 | 2.45 | 2.12 | 2.49 | 2.37 | 1.05 | 1.96 | 1.21 | 2.28 | 2.35 | 2.10 | 2.10 |
| Total | 101.42 | 99.99 | 101.55 | 103.70 | 101.83 | 100.39 | 101.63 | 100.98 | 101.06 | 100.23 | 99.15 | 100.83 | 101.34 | 101.18 | 98.01 | 100.08 | 99.46 | 100.43 | 100.47 | 100.99 | 100.99 |
| *Formula calculated to 12.5 (O)* | | | | | | | | | | | | | | | | | | | | | |
| Na | 0.024 | 0.160 | 0.037 | 0.017 | 0.125 | 0.105 | 0.092 | 0.078 | 0.076 | 0.079 | 0.039 | 0.069 | 0.204 | 0.121 | 0.056 | 0.100 | 0.080 | 0.138 | 0.199 | 0.119 | 0.112 |
| Si | 0.075 | | 0.005 | | | 0.001 | | 0.001 | | | | | | | | | | | | | |
| P | 2.951 | 3.018 | 3.037 | 3.039 | 3.021 | 2.951 | 2.959 | 2.956 | 2.931 | 2.910 | 2.970 | 3.025 | 2.985 | 3.032 | 2.970 | 3.030 | 2.969 | 2.975 | 2.995 | 3.032 | 3.031 |
| Ca | 4.796 | 4.632 | 4.755 | 4.782 | 4.649 | 4.842 | 4.855 | 4.903 | 4.941 | 5.009 | 4.864 | 4.779 | 4.520 | 4.702 | 4.958 | 4.721 | 4.937 | 4.848 | 4.562 | 4.690 | 4.699 |
| Mn | | | | | | 0.001 | | | 0.014 | 0.004 | | | | | | | | | | | |
| Fe | 0.007 | | | | | 0.001 | | 0.003 | 0.009 | 0.020 | 0.101 | | | | | 0.011 | | 0.008 | | | |
| Sr | 0.030 | 0.110 | 0.099 | 0.112 | 0.135 | 0.084 | 0.077 | 0.070 | 0.069 | 0.062 | 0.081 | 0.125 | 0.132 | 0.065 | 0.089 | 0.091 | 0.100 | 0.062 | 0.152 | 0.068 | 0.079 |
| Y | 0.005 | 0.076 | | | 0.036 | 0.025 | 0.050 | 0.040 | 0.046 | 0.040 | 0.007 | | 0.170 | 0.055 | | | | 0.018 | 0.050 | 0.031 | 0.039 |
| La | 0.011 | | | | | 0.004 | 0.002 | 0.000 | 0.001 | 0.001 | | | | | | | | | | | |
| Ce | 0.028 | 0.013 | | | | 0.011 | 0.006 | 0.005 | 0.002 | 0.003 | | | | 0.007 | | 0.016 | | | 0.012 | 0.038 | 0.020 |
| Pr | | | | | | 0.002 | 0.001 | 0.001 | 0.002 | 0.000 | | | | | | | | | | | |
| Nd | | | | | | 0.011 | 0.007 | 0.007 | 0.003 | 0.004 | | | | | | | | | | | |
| Sm | | | | | | 0.001 | 0.001 | | | | | | | | | | | | | | |
| Gd | | | | | | 0.005 | 0.005 | 0.005 | 0.004 | 0.003 | | | | | | | | | | | |
| Dy | | | | | | 0.003 | 0.005 | 0.004 | 0.004 | 0.004 | | | | | | | | | | | |
| S | 0.020 | | 0.008 | | 0.016 | 0.016 | 0.003 | 0.001 | 0.003 | 0.003 | | | 0.010 | | | 0.010 | | 0.016 | 0.035 | | |
| F | 1.481 | 1.687 | 1.543 | 1.504 | 1.558 | 1.375 | 1.231 | 1.348 | 1.280 | 1.366 | 1.600 | 1.348 | 1.606 | 1.505 | 0.733 | 1.250 | 0.846 | 1.456 | 1.515 | 1.332 | 1.278 |
| Cl | | | | | | 0.001 | | 0.001 | | | | | | | | | | | | | |
| Ca site | 4.901 | 4.990 | 4.892 | 4.912 | 4.945 | 5.094 | 5.101 | 5.115 | 5.172 | 5.230 | 5.091 | 4.972 | 5.026 | 4.950 | 5.103 | 4.938 | 5.117 | 5.074 | 4.975 | 4.945 | 4.950 |
| P site | 3.046 | 3.018 | 3.050 | 3.039 | 3.037 | 2.968 | 2.962 | 2.957 | 2.933 | 2.912 | 2.970 | 3.025 | 2.994 | 3.032 | 2.970 | 3.040 | 2.969 | 2.991 | 3.031 | 3.032 | 3.031 |
| F site | 1.481 | 1.687 | 1.543 | 1.504 | 1.558 | 1.377 | 1.231 | 1.349 | 1.280 | 1.366 | 1.600 | 1.348 | 1.606 | 1.505 | 0.733 | 1.250 | 0.846 | 1.456 | 1.515 | 1.332 | 1.278 |

Notes: – denotes elements below LOD. Blank cells denote elements not analysed. *Analysed at NHM; all other analyses carried out at BGS. F results are non-stoichiometric and should only be interpreted as indicating a fluorapatite composition.

**Table 3**
Average apatite trace element concentrations. Full dataset available in the Supplementary information.

| Apatite type | Ap-0, Fenite | | Ap-1, C1 | | Ap-2, C1 | | Ap-3, C2 | | Ap-3, C2 | | Ap-3, C2 | | Ap-3, C2 | | Ap-3, C2 | | Ap-3, C2 | | Ap-3, C2 | | Ap-3, C2 | |
|---|---|---|---|---|---|---|---|---|---|---|---|---|---|---|---|---|---|---|---|---|---|---|
| Sample | T0134 | | T0218 | | T0218 | | T0324* | | T0206 | | T0202 | | T0322* | | T0234 | | T0232 | | T0225 | | | |
| | $n = 8$ | 2SD | $n = 23$ | 2SD | $n = 15$ | 2SD | $n = 11$ | 2SD | $n = 2$ | 2SD | $n = 7$ | 2SD | $n = 15$ | 2SD | $n = 5$ | 2SD | $n = 2$ | 2SD | $n = 6$ | 2SD | | |
| Na | | | 1100 | 140 | 950 | 56 | | | 2900 | 2200 | 5000 | 1000 | | | 3700 | 480 | | | | | | |
| Mg | | | 30 | 10 | 21 | 2 | | | 180 | 190 | 14 | 2 | | | 91 | 89 | | | | | | |
| Mn | | | 270 | 16 | 280 | 36 | | | 170 | 53 | 97 | 22 | | | 140 | 57 | | | | | | |
| Fe | | | 120 | 36 | 140 | 65 | | | 510 | 640 | 530 | 360 | | | 2000 | 1000 | | | | | | |
| As | | | 12 | 1 | 10 | 2 | n.a. | n.a. | 5 | 1 | 19 | 4 | n.a. | n.a. | 14 | 3 | n.a. | n.a. | n.a. | n.a. | | |
| Sr | 940 | 67 | 13,000 | 480 | 14,000 | 850 | 8600 | 1200 | 13,000 | 3100 | 14,000 | 920 | 11,000 | 890 | 13,000 | 1500 | 11,000 | 500 | 19,000 | 920 | | |
| Y | 920 | 55 | 290 | 100 | 380 | 95 | 6600 | 940 | 6900 | 6500 | 12,000 | 3400 | 7300 | 830 | 6100 | 590 | 10,000 | 70 | 5400 | 1200 | | |
| Ba | 28 | 32 | 39 | 10 | 36 | 10 | 97 | 54 | 79 | 11 | 120 | 78 | 95 | 15 | 88 | 25 | 160 | 80 | 170 | 9 | | |
| La | 2900 | 490 | 950 | 64 | 1100 | 120 | 220 | 57 | 420 | 550 | 370 | 56 | 450 | 110 | 630 | 260 | 970 | 49 | 850 | 260 | | |
| Ce | 6200 | 650 | 1500 | 110 | 1900 | 150 | 820 | 190 | 870 | 750 | 1200 | 150 | 1300 | 200 | 2500 | 710 | 3500 | 90 | 2300 | 390 | | |
| Pr | 790 | 72 | 160 | 9 | 180 | 15 | 150 | 32 | 100 | 48 | 200 | 28 | 240 | 31 | 450 | 120 | 660 | 27 | 380 | 34 | | |
| Nd | 3400 | 180 | 530 | 34 | 620 | 38 | 840 | 180 | 480 | 75 | 1200 | 230 | 1400 | 170 | 2700 | 740 | 3800 | 300 | 2300 | 320 | | |
| Sm | 500 | 25 | 81 | 7 | 95 | 7 | 370 | 73 | 230 | 100 | 650 | 100 | 610 | 80 | 890 | 170 | 1400 | 52 | 950 | 280 | | |
| Eu | 77 | 8 | 28 | 4 | 33 | 4 | 180 | 32 | 150 | 79 | 330 | 49 | 280 | 35 | 350 | 55 | 570 | 32 | 420 | 130 | | |
| Gd | 390 | 27 | 82 | 17 | 110 | 17 | 740 | 130 | 560 | 350 | 1200 | 190 | 1100 | 130 | 1000 | 130 | 1800 | 70 | 1400 | 420 | | |
| Tb | 42 | 3 | 14 | 5 | 19 | 5 | 160 | 25 | 130 | 95 | 260 | 49 | 210 | 25 | 180 | 17 | 340 | 3 | 250 | 69 | | |
| Dy | 200 | 11 | 71 | 23 | 100 | 26 | 1200 | 180 | 980 | 930 | 2000 | 430 | 1400 | 160 | 1100 | 110 | 2100 | 32 | 1300 | 360 | | |
| Ho | 34 | 3 | 12 | 4 | 16 | 4 | 240 | 34 | 240 | 240 | 430 | 110 | 270 | 31 | 220 | 20 | 400 | 5 | 240 | 56 | | |
| Er | 82 | 9 | 25 | 9 | 32 | 8 | 570 | 78 | 640 | 620 | 1100 | 320 | 630 | 71 | 540 | 58 | 900 | 25 | 480 | 95 | | |
| Tm | 9 | 1 | 3 | 1 | 3 | 1 | 58 | 7 | 72 | 66 | 120 | 36 | 67 | 7 | 62 | 7 | 94 | 3 | 50 | 7 | | |
| Yb | 52 | 7 | 14 | 6 | 16 | 4 | 270 | 29 | 320 | 280 | 530 | 140 | 290 | 30 | 310 | 38 | 430 | 21 | 220 | 22 | | |
| Lu | 7 | 1 | 1 | 1 | 2 | <1 | 25 | 3 | 40 | 35 | 50 | 13 | 27 | 3 | 32 | 4 | 48 | 1 | 23 | 2 | | |
| Pb | 8 | 1 | 3 | <1 | 4 | 1 | 42 | 16 | 19 | 25 | 19 | 4 | 10 | 1 | 28 | 4 | 32 | 3 | 50 | 10 | | |
| Th | 96 | 11 | 16 | 4 | 23 | 8 | 360 | 39 | 260 | 360 | 630 | 180 | 270 | 32 | 620 | 180 | 770 | 23 | 3000 | 920 | | |
| U | 14 | 2 | 1 | <1 | 2 | 1 | 15 | 4 | 22 | 41 | 39 | 23 | b.d. | b.d. | 19 | 12 | 3 | <1 | 20 | 9 | | |

| Apatite type | Ap-3, C3 | | Ap-3, C3 | | Ap-3, C3 | | Ap-3, C3 | | Ap-3, C3 | | Ap-4 | | Ap-4 | | Ap-4 | | Ap-3, Mn-Fe-V | |
|---|---|---|---|---|---|---|---|---|---|---|---|---|---|---|---|---|---|---|
| Sample | T0327* | | T0262 | | U4904 | | T0167 | | T0317* | | U4909 | | T0134 | | T0178C | | T0227 & U4927 | |
| | $n = 16$ | 2SD | $n = 6$ | 2SD | $n = 8$ | 2SD | $n = 23$ | 2SD | $n = 11$ | 2SD | $n = 14$ | 2SD | $n = 3$ | 2SD | $n = 4$ | 2SD | $n = 13$ | 2SD |
| Na | | | 1900 | 250 | 3400 | 360 | 2400 | 200 | | | 4500 | 180 | 4400 | 740 | | | 4500 | 310 |
| Mg | | | 82 | 67 | 170 | 130 | 25 | 14 | | | 130 | 57 | 89 | 35 | | | 46 | 11 |
| Mn | | | 220 | 110 | 510 | 78 | 140 | 17 | | | 210 | 24 | 210 | 53 | | | 380 | 44 |
| Fe | | | 1000 | 530 | 670 | 270 | 190 | 230 | | | 1900 | 540 | 1300 | 480 | | | 620 | 270 |
| As | n.a. | n.a. | 7 | 2 | 13 | 1 | 6 | 1 | n.a. | n.a. | 4 | 1 | n.a. | n.a. | n.a. | n.a. | 15 | 1 |
| Sr | 13,000 | 740 | 11,000 | 800 | 11,000 | 860 | 11,000 | 490 | 9900 | 1700 | 12,000 | 1800 | 12,000 | 1200 | 11,000 | 2300 | 9400 | 530 |
| Y | 4200 | 290 | 2100 | 340 | 3300 | 240 | 5000 | 400 | 4800 | 560 | 5100 | 760 | 5500 | 1300 | 8100 | 4400 | 6500 | 550 |
| Ba | 76 | 15 | 140 | 40 | 87 | 7 | 69 | 7 | 160 | 41 | 100 | 14 | 190 | 47 | 85 | 16 | 120 | 13 |
| La | 1000 | 78 | 320 | 55 | 1000 | 230 | 330 | 34 | 1400 | 210 | 280 | 120 | 290 | 83 | 430 | 180 | 1300 | 130 |
| Ce | 3000 | 250 | 1100 | 83 | 3200 | 590 | 1200 | 140 | 4000 | 500 | 870 | 390 | 690 | 220 | 890 | 380 | 4200 | 370 |
| Pr | 480 | 43 | 190 | 21 | 430 | 68 | 220 | 22 | 630 | 75 | 120 | 56 | 96 | 46 | 110 | 49 | 620 | 59 |
| Nd | 2500 | 240 | 1200 | 280 | 1900 | 230 | 1200 | 120 | 3000 | 390 | 630 | 280 | 520 | 290 | 500 | 240 | 3100 | 340 |
| Sm | 760 | 69 | 410 | 130 | 550 | 47 | 420 | 43 | 920 | 130 | 280 | 110 | 220 | 150 | 220 | 120 | 760 | 81 |
| Eu | 270 | 22 | 160 | 50 | 200 | 12 | 170 | 17 | 330 | 42 | 170 | 65 | 130 | 76 | 140 | 75 | 310 | 31 |
| Gd | 870 | 76 | 470 | 150 | 620 | 53 | 480 | 52 | 1100 | 140 | 690 | 250 | 530 | 270 | 710 | 410 | 930 | 95 |
| Tb | 140 | 12 | 71 | 19 | 100 | 7 | 93 | 9 | 180 | 24 | 180 | 55 | 130 | 52 | 220 | 130 | 170 | 18 |
| Dy | 910 | 70 | 400 | 85 | 610 | 46 | 650 | 63 | 1200 | 140 | 1100 | 280 | 970 | 320 | 1600 | 900 | 1100 | 92 |
| Ho | 160 | 12 | 73 | 13 | 130 | 10 | 150 | 14 | 210 | 24 | 200 | 38 | 200 | 60 | 310 | 160 | 210 | 23 |
| Er | 410 | 28 | 190 | 27 | 280 | 19 | 440 | 38 | 470 | 52 | 430 | 61 | 490 | 120 | 660 | 330 | 580 | 68 |
| Tm | 53 | 3 | 24 | 2 | 39 | 3 | 62 | 5 | 49 | 5 | 48 | 6 | 62 | 16 | 75 | 36 | 80 | 8 |
| Yb | 280 | 18 | 130 | 12 | 190 | 14 | 320 | 22 | 210 | 22 | 270 | 29 | 340 | 74 | 370 | 150 | 480 | 67 |
| Lu | 32 | 2 | 14 | 1 | 24 | 2 | 34 | 2 | 20 | 2 | 31 | 3 | 38 | 7 | 41 | 14 | 55 | 7 |
| Pb | 19 | 1 | 25 | 2 | 16 | 3 | 16 | 1 | 75 | 27 | 61 | 9 | 55 | 10 | 67 | 11 | 35 | 4 |
| Th | 460 | 42 | 620 | 240 | 290 | 29 | 270 | 38 | 370 | 79 | 580 | 100 | 780 | 300 | 910 | 170 | 1300 | 230 |
| U | 1 | <1 | 1 | 1 | 6 | 1 | 11 | 1 | 1 | <1 | 27 | 5 | 72 | 20 | 30 | 5 | 12 | 2 |

Notes: Blank cells denote elements with a high blank concentration; n.a. = not analysed; b.d. = below detection; *analysed at Aberystwyth, all other analyses undertaken at the BGS.

### 4.4. LREE minerals (C2, C3—main Songwe carbonatite)

Ap-3 bands are truncated by a LREE-bearing mineral assemblage (e.g. Fig. 6C), providing clear evidence of later LREE crystallisation. The LREE assemblage is dominated by the fluorocarbonate, synchysite-(Ce), with very minor parisite-(Ce) and, locally, florencite-(Ce). Synchysite-(Ce) occurs as randomly orientated laths or tabular crystals and/or fibroradial to plumose aggregates (Fig. 9). The crystal size varies between 10 μm to 60 μm while crystal aggregates can reach up to 400 μm. Strontianite and/or baryte also occur in the LREE mineral assemblage, either as inclusions and/or intergrowths, forming distinctive vein-like aggregates or segregations (Fig. 9B). In addition, synchysite-(Ce) is locally associated with calcite, fluorite and K-feldspar.

Cross-cutting relationships clearly indicate that synchysite-(± parisite)-baryte-strontianite crystallisation occurs after Ap-3 crystallisation. Such LREE mineral assemblages are typical of late-stage hydrothermal REE mineralisation in carbonatites (Mariano, 1989). This mineralisation can occur as hexagonal pseudomorphs, most likely

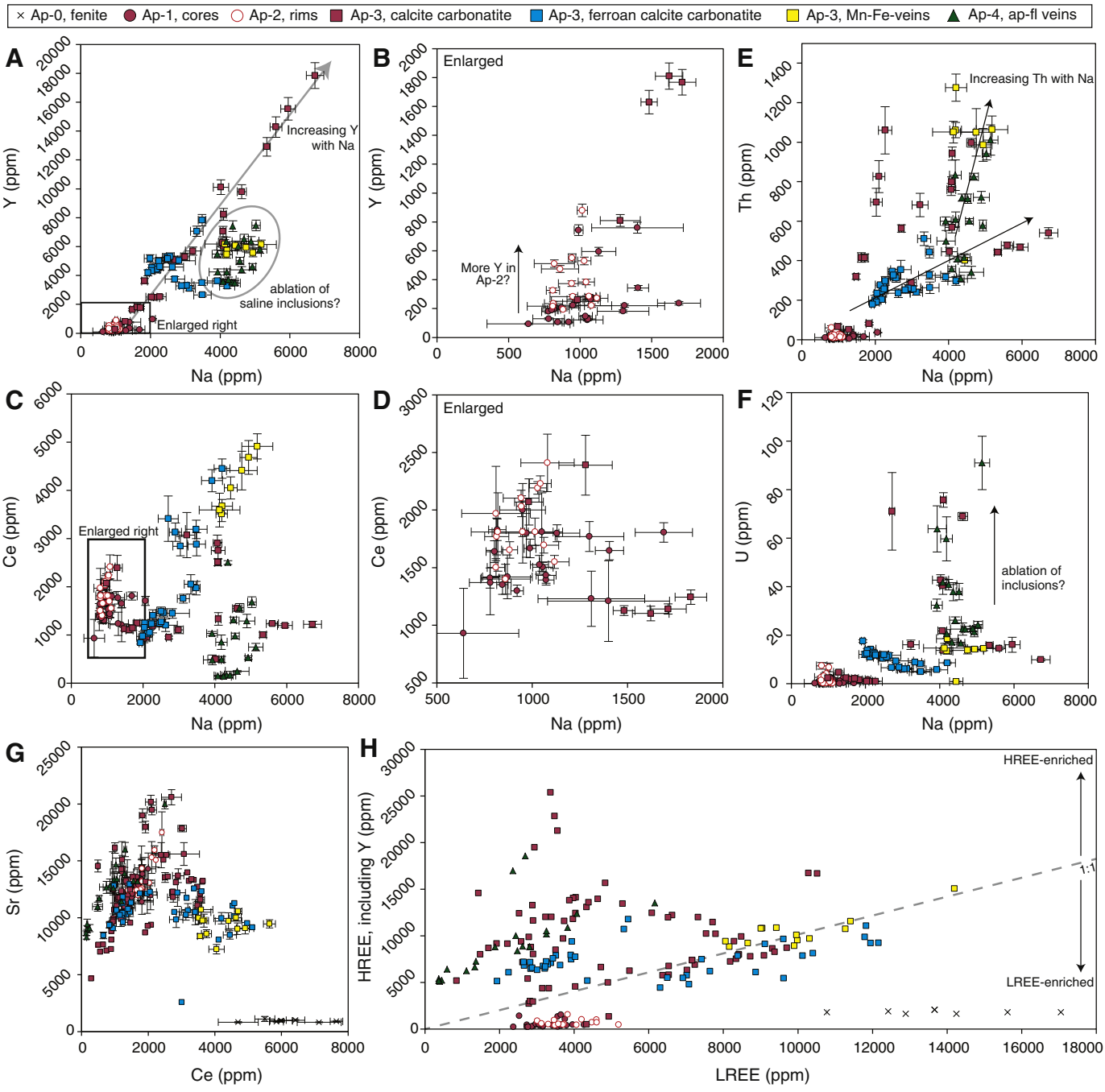


**Fig. 3.** Variation in REE and trace element concentrations in Songwe apatite from LA-ICP-MS data. Error bars represent 2 standard errors derived for each integration.

after burbankite (Wall and Mariano, 1996; Zaitsev et al., 2002; Wall and Zaitsev, 2004; Moore et al., 2015). However, at Songwe, the assemblage occurs along fractures, in small cavities or is widespread, and pseudomorphs are not apparent, akin to similar descriptions at Barra do Itapirapuã and Amba Dongar (Andrade et al., 1999; Doroshkevich et al., 2009).

Florencite-(Ce) is particularly abundant in the groundmass of feldspar-rich samples, forming narrow acicular crystals (<20 μm in width), and is associated with Fe- and Mn-bearing oxides. Locally, it also occurs as small anhedral crystals along the edges of entrained carbonate in apatite veins, most likely forming a replacement/alteration product of apatite. There is little consistent compositional variation between different florencite-(Ce) and synchysite-(Ce) samples (Table 4).

### 4.5. Ap-4 (apatite-fluorite veins)

Ap-4 occurs in apatite-fluorite veins found outside the main carbonatite intrusion at Chenga Hill (Fig. 1B), as well as at depth in drill holes (Broom-Fendley, 2015). It is texturally similar to Ap-3, comprising aggregates of euhedral to subhedral grains, each with a resorbed core and a recrystallised overgrowth (Fig. 10). This apatite type is associated with fluorite, calcite, baryte, quartz and xenotime-(Y). It displays tan–green and purple–white luminescence similar to Ap-3 (Fig. 6) but has a considerably more complex texture in BSE images (Fig. 10). Earlier remnant dark cores are overgrown by bright, spongy apatite, which is commonly overgrown by xenotime-(Y).

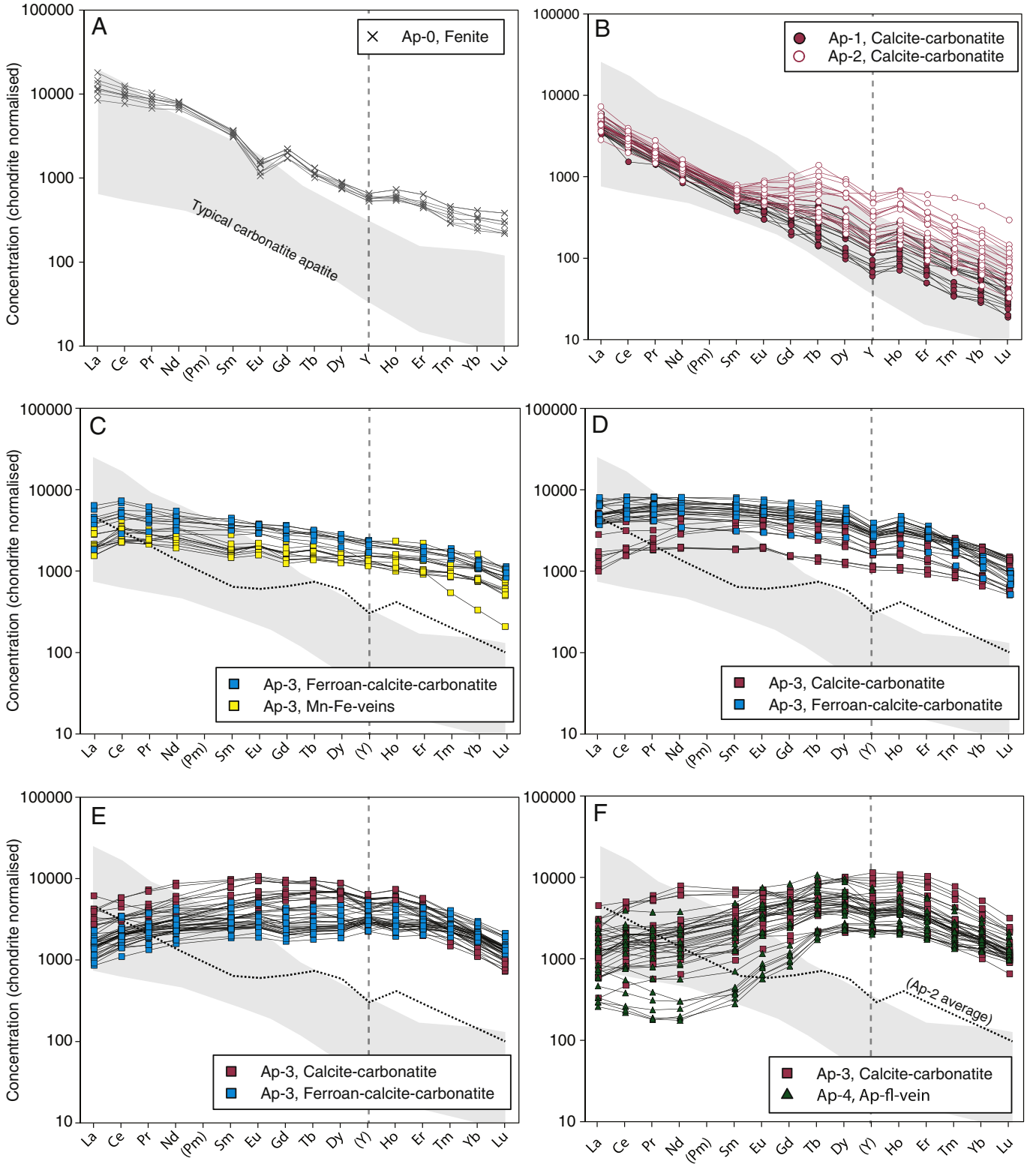


**Fig. 4.** Distribution of REE + Y in fluorapatite from fenite, calcite carbonatite, ferroan calcite carbonatite, Mn-Fe-veins and apatite-fluorite veins. Plots show the most common REE distributions in the apatite from Songwe. Background shaded values represent the range of REE distributions in apatite from other carbonatite complexes, re-plotted after Hornig-Kjarsgaard (1998). The dotted line represents average Ap-2 values, for comparison. REE distributions are normalised using the values of McDonough and Sun (1995).

Ap-4 is compositionally similar to Ap-3 but Na, Sr, U and REE concentrations are among the highest of all the apatite analysed (Fig. 3). Na and Y are positively related, while Ce and Na show a weak relationship. The REE distribution of Ap-4 is LREE poor and HREE enriched with a small negative Y anomaly (Fig. 4F).

Small fluid inclusions are abundant in Ap-4 but the apatite is commonly turbid and the inclusions are not amenable to study (Fig. 7B). Where inclusions are discernible, they are interpreted as primary on the basis of their elongate habits, and occurrence parallel to grain boundaries. Many inclusions, however, have leaked and few LV

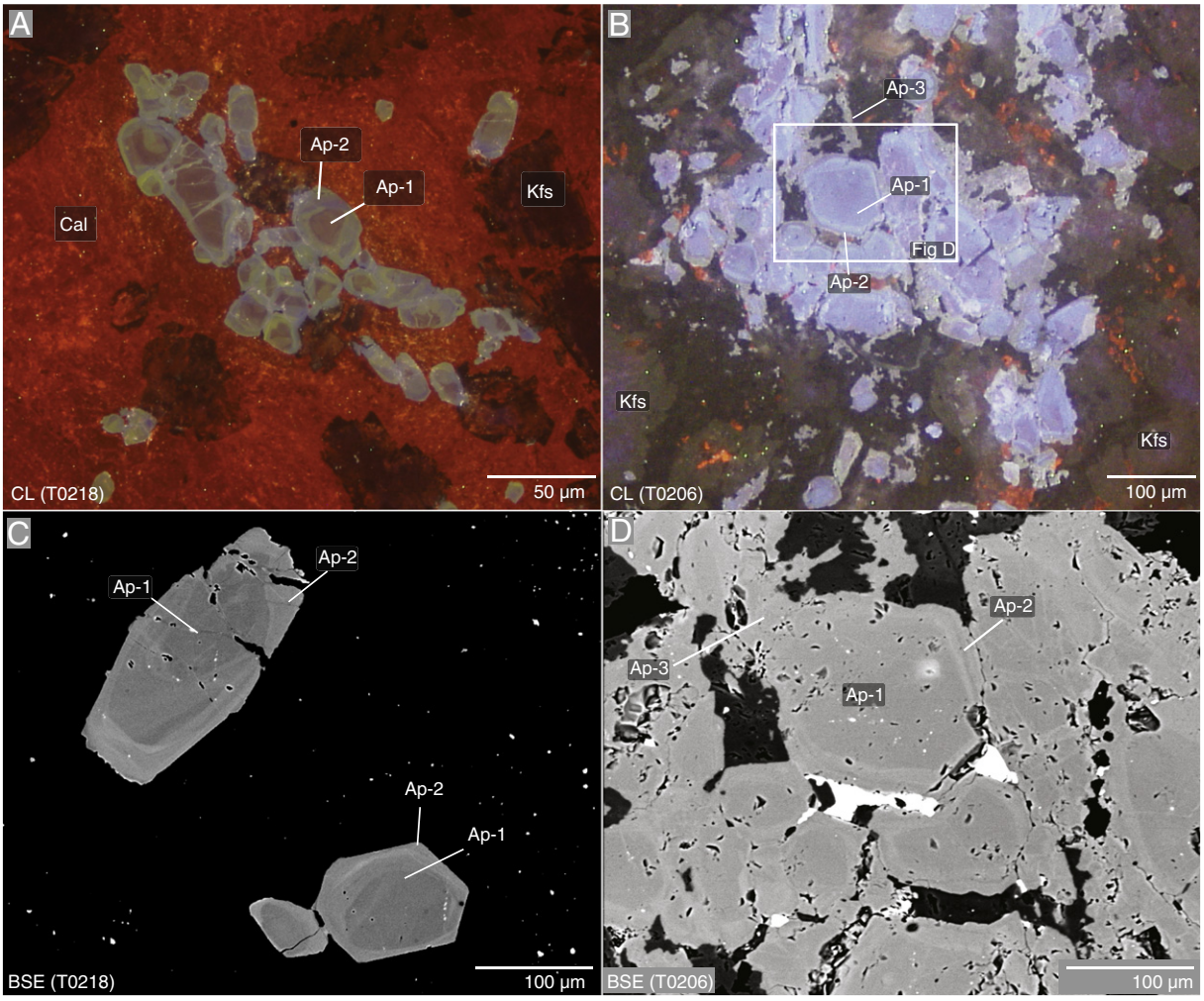


**Fig. 5.** CL (A–B) and BSE (C–D) images of Ap-1, 2 and 3 from C1 calcite carbonatite. Abbreviations same as Fig. 2. Note the rounded/euhedral shape, zoning between Ap-1 and Ap-2, and juxtaposition with Ap-3.

inclusions remain. There are no inclusions with more than two phases and few have a readily visible vapour bubble.

Few microthermometric data are available from Ap-4; no ice melting was observable. Homogenisation temperatures, by disappearance of the vapour phase, ranged between 160–230 °C if a single outlier is excluded (Supplementary data; Fig. 8).

Cross-cutting relationships for Ap-4 and other apatite types are scarce as Ap-4 principally occurs in thin veins outside of the carbonatite. As these veins are associated with fluorite mineralisation, Ap-4 is interpreted to occur late in the paragenetic sequence, as further supported by its lower fluid inclusion homogenisation temperature than Ap-3 (Fig. 8).

### 4.6. Xenotime-(Y) (apatite-fluorite veins)

Minor xenotime-(Y) crystallisation follows the formation of Ap-4 in the apatite-fluorite veins at Chenga Hill. Xenotime-(Y) occurs in two habits, both of which are synchronous with recrystallised calcite and are commonly found in association with fluorite:

1. Xenotime-(Y) associated with fine-grained bands of rutile, zircon and Fe-oxides, and fenite clasts (Fig. 11A). This xenotime type is small (up to 10 μm across) and uncommon, accounting for approximately 5% of the xenotime present. It is associated with euhedral Fe-oxides, subhedral rutile and disseminated zircon. The xenotime commonly overgrows zircon and/or rutile, but also forms solitary euhedral crystals.

2. Xenotime-(Y) occurring as overgrowths on apatite (Fig. 11B). This xenotime type is larger (up to 50 μm across) and the most abundant (approximately 95 modal % of the xenotime present). It exhibits fine oscillatory zones, with a small rutile core and a spongy Zr-rich phase.

Compositionally, the two xenotime types are similar (Table 5; Fig. 12A–B). Only $UO_2$ and $ThO_2$ vary, and are slightly more concentrated in xenotime overgrowing apatite, although this is clearer for $ThO_2$ than for $UO_2$ as $UO_2$ concentrations show a large degree of scatter. There is no difference between the REE distributions of the xenotime types. Both are enriched in HREE, peaking at Y and with no Y or Eu anomalies (Fig. 12B).

### 4.7. Fluorite (apatite-fluorite veins)

Extensive fluorite mineralisation is associated with Ap-4 in the apatite-fluorite veins. Fluorite is anhedral and crystallises after Ap-4. It occurs as stringers or as discreet patches, and is commonly associated with bright orange-luminescent calcite.

Fluorite was analysed from fluid inclusion-poor areas of an apatite-fluorite vein sample (U4909). The concentrations of most trace elements, including the REE, are low compared to those in apatite and there is little correlation between the different elements (Table 6). REE contents total <1000 ppm, of which most (>500 ppm) is Y, corresponding with a positive Y anomaly on chondrite-normalised REE diagrams (Fig. 13). Fluorite is depleted in the LREE, and is HREE-enriched.

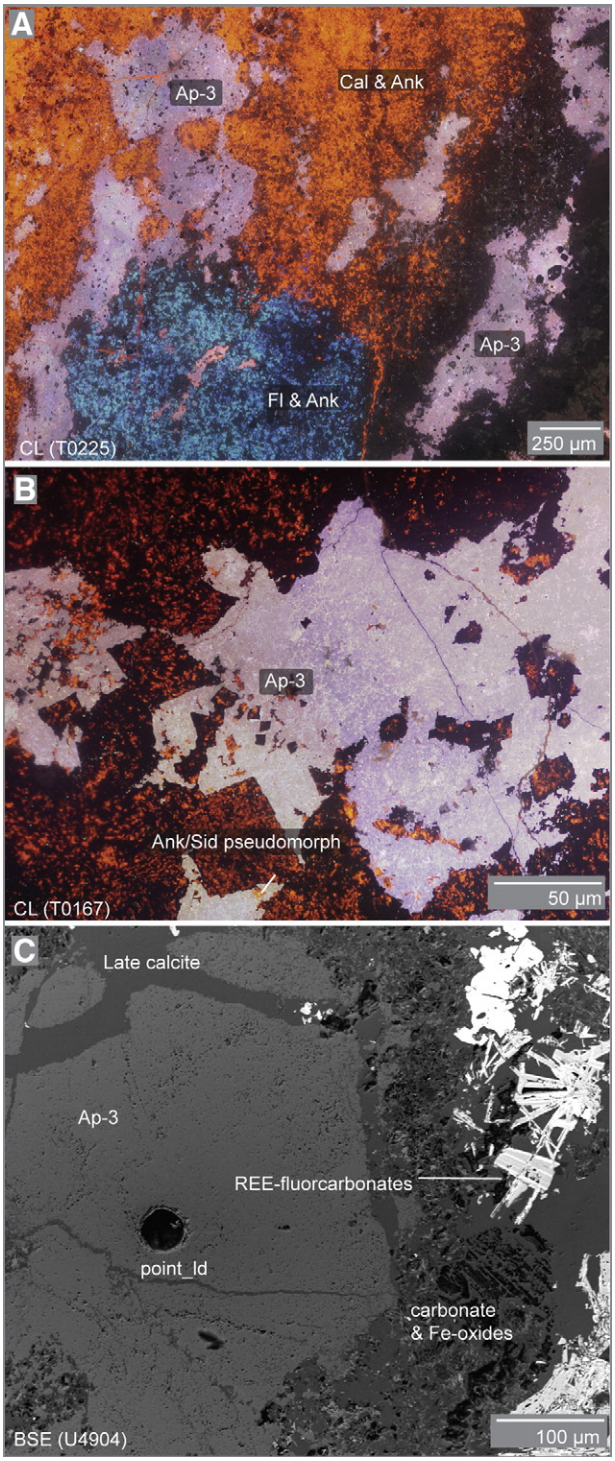


**Fig. 6.** CL (A–B) and BSE (C) images of Ap-3 from C2 calcite carbonatite (A) and C3 Ferroan calcite carbonatite (B–C). Abbreviations same as Fig. 2 plus Ank, ankerite; Sid, siderite.

With the exception of the Y anomaly, the REE pattern is similar to that of Ap-4, except an order of magnitude lower.

Fluorite contains many simple LV fluid inclusions that are interpreted as primary on the basis of uniform vapour volumes (15–20%), negative mineral shapes and random distribution within the host mineral grain (Fig. 7C). A small number of inclusions also contained a trapped, highly birefringent, mineral, interpreted as a carbonate.

Microthermometric data were acquired from 44 inclusions (Supplementary data). Homogenisation temperatures to liquid ranged between

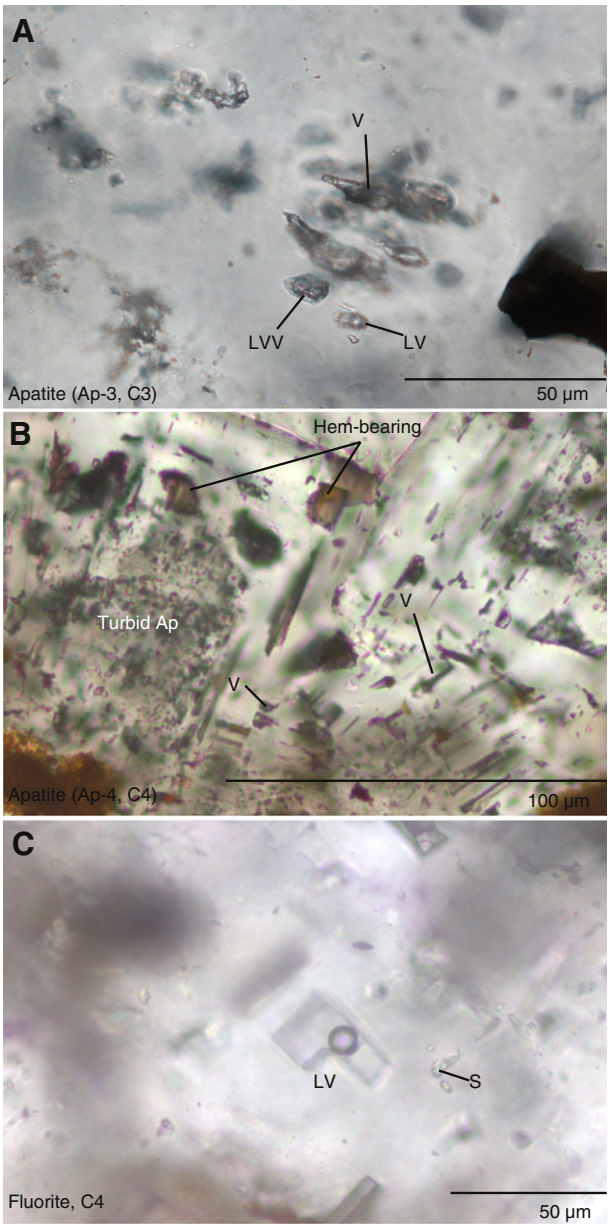


**Fig. 7.** Images of fluid inclusions in (A) Ap-3, (B) Ap-4, and (C) fluorite from (A) C3 carbonatites and (B–C) apatite-fluorite veins. L, liquid; V, vapour; S, solid; Hem, hematite.

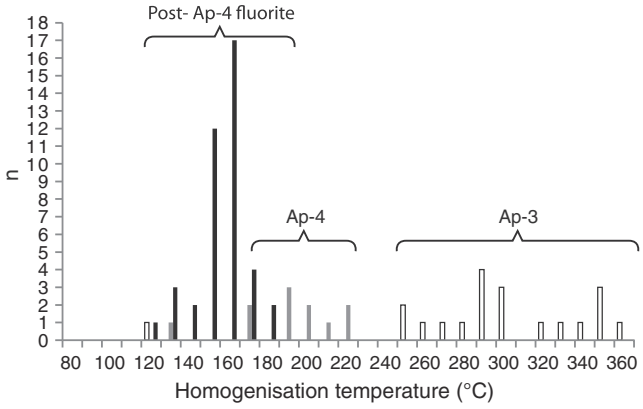


**Fig. 8.** Histogram of homogenisation temperatures of fluid inclusions in apatite (Ap-3 and Ap-4) and fluorite in C3 carbonatite and apatite fluorite veins carbonatites at Songwe.

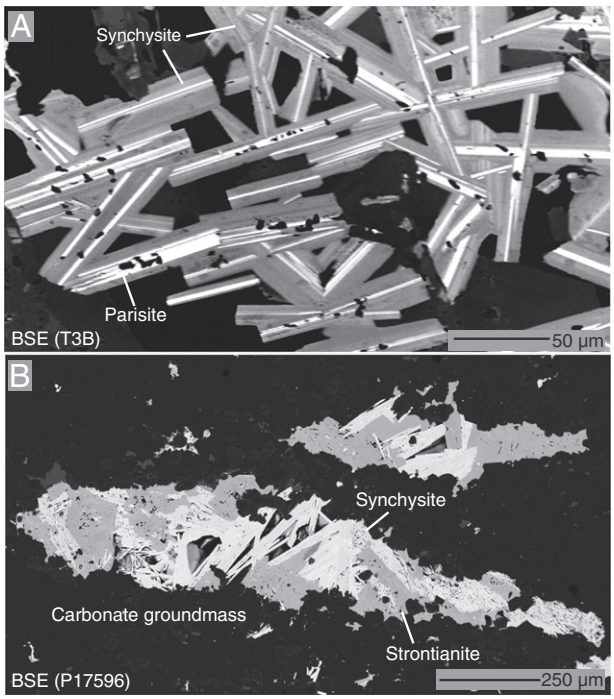


**Fig. 9.** BSE images of LREE minerals at Songwe: (A) syntaxial intergrowths of synchysite-(Ce) and (brighter) parisite-(Ce); and (B) clusters of synchysite-(Ce) associated with strontianite and baryte.

120–170 °C (median 151 °C; Fig. 8) and final ice melting temperatures between −8.6 and −0.3 °C. These temperatures correspond to a salinity range of 0.5–12.5 wt% NaCl, assuming a pure NaCl composition (Bodnar, 1993). Heating of the sample was aborted after 170 °C to reduce the impact of leakage; consequently one data point does not have a homogenisation temperature. Decrepitation also occurred in some samples; this took place after homogenisation, but meant fewer melting temperatures were acquired.

Fluorite is interpreted as one of the last minerals to crystallise at Songwe, which is common in many carbonatites (Simonetti and Bell, 1995; Palmer and Williams-Jones, 1996; Williams-Jones and Palmer, 2002). After fluorite mineralisation, late-stage quartz crystallisation occurs, followed by alteration of the carbonatite by low-T late fluids (Fig. 2).

## 5. Discussion

### *5.1. Comparison with REE-bearing minerals from other localities and rock types*

#### *5.1.1. Apatite*

It is evident from this study that most apatite at Songwe is HREE-enriched and crystallisation occurred late in the carbonatite evolution. For comparison with apatite from other localities, a database of apatite compositions has been compiled (Supplementary information). This database comprises apatite compositions from carbonatites and granitoids and incorporates previously published discrimination diagrams (Hogarth, 1989; Belousova et al., 2002). Data, however, are primarily obtained from LA ICP-MS and large EPMA datasets have been excluded (e.g. Fleischer and Altschuler, 1986). A brief discussion on the comparability of these datasets is available in the Supplementary information. Studies of late-stage apatite in carbonatites are less common (Ngwenya, 1994; Wall and Mariano, 1996; Walter et al., 1995). However, recently published LA ICP-MS data are available for late-stage, HREE-enriched, apatite from the Kangankunde and Tundulu carbonatites, Malawi (Broom-Fendley et al., 2016a). This allows some geochemical comparison with Songwe apatite.

Compositionally, all the apatite data from Songwe plot in the carbonatite Mn–Sr field (after Hogarth, 1989 and Belousova et al., 2002; Fig. 14A), reaffirming the apatite is carbonatite-derived. Fenite apatite compositions from Songwe, with just 1000 ppm Sr, are an exception to this but Mn analyses have poor accuracy and are not plotted. When compared using a Y–Sr diagram (Fig. 14B), Songwe apatite plots outside the carbonatite field of Belousova et al. (2002); Ap-0 from fenite has a more granitoid-like composition and Ap-3 and Ap-4 have much higher Y concentrations than other carbonatite-apatite analyses. This pattern is also clear where Y and La are used for comparison of REE concentrations (Fig. 14C): Ap-3 and Ap-4 have Y concentrations similar to, or higher than, apatite from granitoids. Y concentrations are higher than apatite from Tundulu and Kangankunde, indicating that apatite at Songwe has the highest published HREE concentrations of any carbonatite-derived apatite within the bounds of our literature search.

Regardless of their similar HREE-enrichment, apatite from Songwe differs texturally to apatite from Tundulu and Kangankunde: core–rim overgrowths are readily identifiable in apatite from these carbonatites but are absent in Ap-3 from Songwe. Mineral associations, too, are dissimilar: at Kangankunde and Tundulu, quartz is associated with the late apatite overgrowths, but at Songwe quartz is uncommon. Extensive calcite is associated with the apatite at Songwe, but very little carbonate occurs with late-stage apatite at Kangankunde or Tundulu. Apatite crystallisation at both Songwe and Tundulu, however, precedes REE-fluorocarbonate mineralisation. Ap-3 appears to be most texturally similar to the fine-grained, anhedral apatite at Sukulu, Uganda (Ting et al., 1994). While no HREE data are available for apatite from this intrusion, it does display high $Na_2O$, $REE_2O_3$ and SrO concentrations.

#### *5.1.2. Xenotime*

Xenotime is an uncommon phase in carbonatites and only xenotime-(Y) from Kangankunde has formed in a late-stage environment similar to that at Songwe. Wall and Mariano (1996) analysed Kangankunde xenotime using EPMA, permitting comparison with Songwe. Kangankunde xenotime is MREE enriched, peaking at Tb, while xenotime from Songwe has a more typical REE distribution, centred on Y (Fig. 12). Wall and Mariano (1996) interpreted the unusual distribution at Kangankunde as a function of the partition coefficients of apatite and xenotime co-crystallising from an MREE-rich fluid. Texturally, however, xenotime overgrowths on apatite at Songwe appear to have formed after the apatite, and therefore co-crystallisation is unlikely. Instead, xenotime at Songwe may have formed from a late HREE-rich fluid phase, associated with the fluorite mineralisation. Carbonatitic xenotime from Songwe, Kangankunde (Wall and Mariano, 1996) and Lofdal (Wall et al., 2008) does not display an Eu-anomaly, in contrast to xenotime from granitic rocks (e.g. Förster, 1998).

#### *5.1.3. Fluorite*

Fluorite, like apatite, readily accommodates the REE and can be used to trace the REE distribution of fluorite-forming fluids (e.g. Gagnon et al., 2003; Schwinn and Markl, 2005; Xu et al., 2012). Almost all fluorite from carbonatite displays a positive Y anomaly (Bühn et al., 2003; Xu et al., 2012). For example, fluorite REE distributions at Okorusu, Namibia, have La/Yb (i.e. degree of HREE enrichment) and Y/Ho ratios (magnitude of Y anomaly) which decrease in later fluorite (Bühn et al., 2003, Fig. 15). The composition and REE distribution of fluorite from different carbonatites, however, is varied. Sr contents vary from 1 ppm to 1 wt% and Y concentrations are between 1–1000 ppm (Fig. 15A). LREE enriched distributions are common (e.g. fluorite from Daluxiang, Maoniuping, Bayan Obo and Okorusu), as are roof-shaped MREE enriched distributions (e.g. Lizhuang, Maoniuping). HREE enriched distributions, characterised by their low La/Yb ratios, of the

**Table 4**
Selected synchysite-(Ce) and florencite-(Ce) major element compositions by EPMA.

| Sample no.: | P17593 | P17593 | P17598 | P17598 | P17599 | P17599 | P17589 | P17589 | T0318 | T0318 | T0319 | T0319 | T0319 |
|---|---|---|---|---|---|---|---|---|---|---|---|---|---|
| | Synchysite-(Ce) | | | | | | | | Florencite-(Ce) | | | | |
| $Al_2O_3$ | – | – | – | – | – | – | – | – | 30.32 | 28.26 | 28.97 | 30.42 | 28.29 |
| $P_2O_5$ | – | – | – | – | – | – | – | – | 26.87 | 25.70 | 25.21 | 26.90 | 24.40 |
| $SiO_2$ | 0.07 | 0.07 | 0.04 | 0.06 | 0.09 | 0.14 | 0.07 | 0.10 | 0.14 | 0.36 | 0.25 | 0.16 | 0.17 |
| CaO | 16.63 | 16.96 | 16.72 | 16.63 | 17.15 | 16.49 | 16.18 | 15.37 | 0.51 | 1.09 | 0.34 | 0.28 | 0.61 |
| $Fe_2O_3$ | – | – | – | – | – | – | – | – | 2.12 | 5.85 | 3.55 | 1.53 | 3.14 |
| FeO | 0.72 | 0.69 | – | – | – | 0.21 | 0.60 | 0.31 | – | – | – | – | – |
| SrO | 0.22 | 0.72 | 0.57 | 0.26 | – | 0.15 | 0.27 | 0.61 | 5.50 | 7.54 | 8.20 | 7.37 | 9.03 |
| $Y_2O_3$ | 0.67 | 0.50 | 0.43 | 0.40 | 0.34 | 0.50 | 1.13 | 0.47 | – | – | – | – | – |
| $La_2O_3$ | 14.34 | 15.60 | 19.29 | 15.70 | 11.75 | 12.11 | 15.20 | 15.55 | 6.82 | 7.68 | 5.01 | 5.57 | 5.89 |
| $Ce_2O_3$ | 23.64 | 23.45 | 25.59 | 23.97 | 24.70 | 25.05 | 25.27 | 26.79 | 11.23 | 8.66 | 8.89 | 9.96 | 9.12 |
| $Pr_2O_3$ | 2.22 | 2.02 | 1.96 | 2.38 | 2.76 | 2.65 | 2.32 | 2.35 | 1.95 | 1.59 | 1.50 | 1.72 | 1.55 |
| $Nd_2O_3$ | 7.79 | 6.80 | 4.51 | 7.85 | 9.54 | 9.43 | 6.53 | 6.52 | 2.82 | 1.09 | 2.47 | 2.90 | 2.06 |
| $Sm_2O_3$ | 1.04 | 0.88 | 0.17 | 0.70 | 1.23 | 1.08 | 0.63 | 0.55 | 0.16 | 0.02 | 0.28 | 0.27 | 0.13 |
| $Eu_2O_3$ | 0.17 | 0.21 | – | 0.08 | 0.21 | 0.17 | 0.13 | 0.10 | – | – | – | – | – |
| $Gd_2O_3$ | 0.57 | 0.64 | – | – | 0.35 | 0.22 | 0.25 | – | – | – | 0.07 | 0.10 | 0.01 |
| $Dy_2O_3$ | 0.31 | 0.18 | 0.08 | 0.17 | 0.18 | 0.14 | 0.25 | 0.13 | – | – | – | – | – |
| $ThO_2$ | 0.97 | 1.22 | 0.22 | 1.55 | 0.74 | 0.62 | 0.85 | 0.67 | 0.41 | 0.03 | 0.55 | 0.66 | 0.25 |
| $SO_3$ | – | – | – | – | – | – | – | – | 0.11 | 0.10 | 0.72 | 0.76 | 0.75 |
| F | 4.91 | 4.48 | 5.47 | 4.39 | 4.27 | 4.38 | 4.63 | 5.24 | 1.43 | 1.15 | 1.10 | 0.54 | 1.66 |
| $CO_2$ | 28.00 | 28.00 | 28.00 | 28.00 | 28.00 | 28.00 | 28.00 | 28.00 | – | – | – | – | – |
| Total | 102.33 | 102.55 | 103.11 | 102.32 | 101.37 | 101.41 | 102.54 | 102.26 | 90.39 | 89.12 | 87.11 | 89.14 | 87.06 |
| O≡F | 2.07 | 1.89 | 2.30 | 1.85 | 1.80 | 1.84 | 1.95 | 2.21 | 0.60 | 0.48 | 0.46 | 0.23 | 0.70 |
| Total | 100.26 | 100.66 | 100.80 | 100.46 | 99.57 | 99.56 | 100.58 | 100.05 | 89.79 | 88.64 | 86.65 | 88.91 | 86.36 |
| | Formula calculated to 7 (O) | | | | | | | | Formula calculated to 11 (O) | | | | |
| Al | – | – | – | – | – | – | – | – | 3.039 | 2.902 | 3.003 | 3.030 | 2.991 |
| P | – | – | – | – | – | – | – | – | 1.935 | 1.896 | 1.878 | 1.925 | 1.853 |
| Si | 0.004 | 0.004 | 0.002 | 0.003 | 0.005 | 0.008 | 0.004 | 0.005 | 0.012 | 0.031 | 0.022 | 0.014 | 0.015 |
| Ca | 0.950 | 0.970 | 0.948 | 0.955 | 0.989 | 0.950 | 0.926 | 0.895 | 0.046 | 0.102 | 0.032 | 0.025 | 0.059 |
| Fe | 0.032 | 0.031 | – | – | – | 0.009 | 0.027 | 0.014 | 0.151 | 0.427 | 0.261 | 0.108 | 0.235 |
| Sr | 0.007 | 0.022 | 0.017 | 0.008 | – | 0.005 | 0.008 | 0.019 | 0.271 | 0.381 | 0.418 | 0.361 | 0.470 |
| Y | 0.019 | 0.014 | 0.012 | 0.011 | 0.010 | 0.014 | 0.032 | 0.014 | – | – | – | – | – |
| La | 0.282 | 0.307 | 0.376 | 0.310 | 0.233 | 0.240 | 0.299 | 0.312 | 0.214 | 0.247 | 0.163 | 0.174 | 0.195 |
| Ce | 0.461 | 0.458 | 0.496 | 0.470 | 0.486 | 0.493 | 0.494 | 0.533 | 0.350 | 0.276 | 0.286 | 0.308 | 0.300 |
| Pr | 0.043 | 0.039 | 0.038 | 0.046 | 0.054 | 0.052 | 0.045 | 0.047 | 0.060 | 0.050 | 0.048 | 0.053 | 0.051 |
| Nd | 0.148 | 0.130 | 0.085 | 0.150 | 0.183 | 0.181 | 0.125 | 0.127 | 0.086 | 0.034 | 0.078 | 0.088 | 0.066 |
| Sm | 0.019 | 0.016 | 0.003 | 0.013 | 0.023 | 0.020 | 0.012 | 0.010 | 0.005 | 0.001 | 0.008 | 0.008 | 0.004 |
| Eu | 0.003 | 0.004 | – | 0.001 | 0.004 | 0.003 | 0.002 | 0.002 | – | – | – | – | – |
| Gd | 0.010 | 0.011 | – | – | 0.006 | 0.004 | 0.004 | – | – | – | 0.002 | 0.003 | 0.000 |
| Dy | 0.005 | 0.003 | 0.001 | 0.003 | 0.003 | 0.002 | 0.004 | 0.002 | – | – | – | – | – |
| Th | 0.012 | 0.015 | 0.003 | 0.019 | 0.009 | 0.008 | 0.010 | 0.008 | 0.008 | | 0.011 | 0.013 | 0.005 |
| S | – | – | – | – | – | – | – | – | 0.007 | 0.007 | 0.048 | 0.048 | 0.050 |
| F | 0.828 | 0.756 | 0.915 | 0.744 | 0.727 | 0.745 | 0.782 | 0.901 | 0.075 | 0.061 | 0.058 | 0.028 | 0.087 |

Notes: – = below detection limits; na = not analysed; FeO = total iron. Full dataset available in the Supplementary information. Cl, Na and Mn below detection. Florencite totals below 100% due to OH contribution.

magnitude seen at Songwe, however, have not been observed in fluorite from other carbonatites (Fig. 15).

### *5.2. What can the mineral compositions and fluid-inclusion data tell us about the late-stage fluids at Songwe?*

The high HREE contents of apatite and fluorite, compared with other carbonatites, and the presence of xenotime are testament to the elevated HREE at the later stages of emplacement at Songwe. This is highly unusual in carbonatite, where the rocks and minerals are characteristically LREE rich (e.g. Hornig-Kjarsgaard, 1998). The combined geochemical, fluid inclusion and textural data indicate that this HREE enrichment occurs in a fluid-rich environment. Using the paragenetic information, apatite composition and fluid inclusion data, it is possible to infer some characteristics of this late-stage fluid and the behaviour of the REE during transport and deposition.

The presence of F-bearing minerals, and a positive Y anomaly, provides unequivocal evidence of F in the fluid. Furthermore, high $CO_2$ and Cl activity is supported by the presence of $CO_2$ and NaCl in fluid inclusions, as is common in carbonatite-derived fluid (Rankin, 2005). Magmatic halite from the St Honoré carbonatite also attests to the presence of Cl in carbonatite magmas and, therefore, supports the likelihood of its presence in a carbonatite-derived hydrothermal fluid (Kamenetsky et al., 2015). The predominance of Ca-REE-fluorocarbonates and apatite, as well as the absence of bastnäsite, potentially indicates a high Ca and P activity in the fluid. However, for apatite, incorporation of these elements through reaction with the magmatic carbonatite is likely (e.g. Kasioptas et al., 2008, 2011).

From the fluid inclusion data it is also possible to make some general observations (Fig. 2C):

1. $CO_2$ is only present in inclusions in Ap-3, and a large proportion of the inclusions in this apatite type are vapour rich.
2. The proportion of single-phase vapour inclusions decreases later in the paragenesis.
3. The homogenisation temperature of the inclusions decreases at later stages in the paragenesis.

The presence of $CO_2$ and the saline nature of inclusions in Ap-3 indicates both chloride and carbonate/bicarbonate may have been present in a fluid. In inclusions hosted by Ap-4 and fluorite, however, only chloride can be inferred because of the lack of a $CO_2$ bubble. The

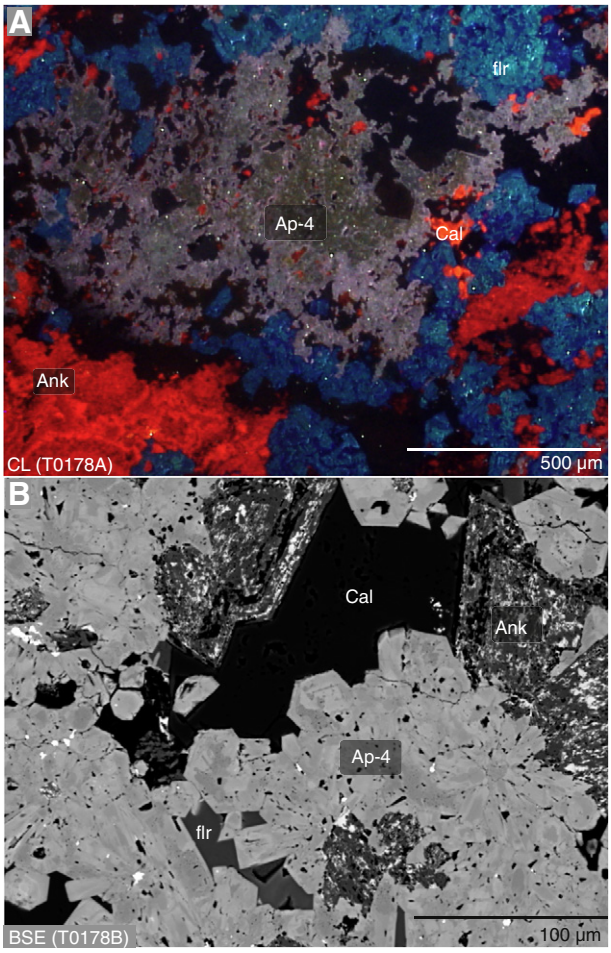


**Fig. 10.** CL (A) and BSE (B) images of Ap-4 from apatite-fluorite veins. Abbreviations same as Fig. 2.

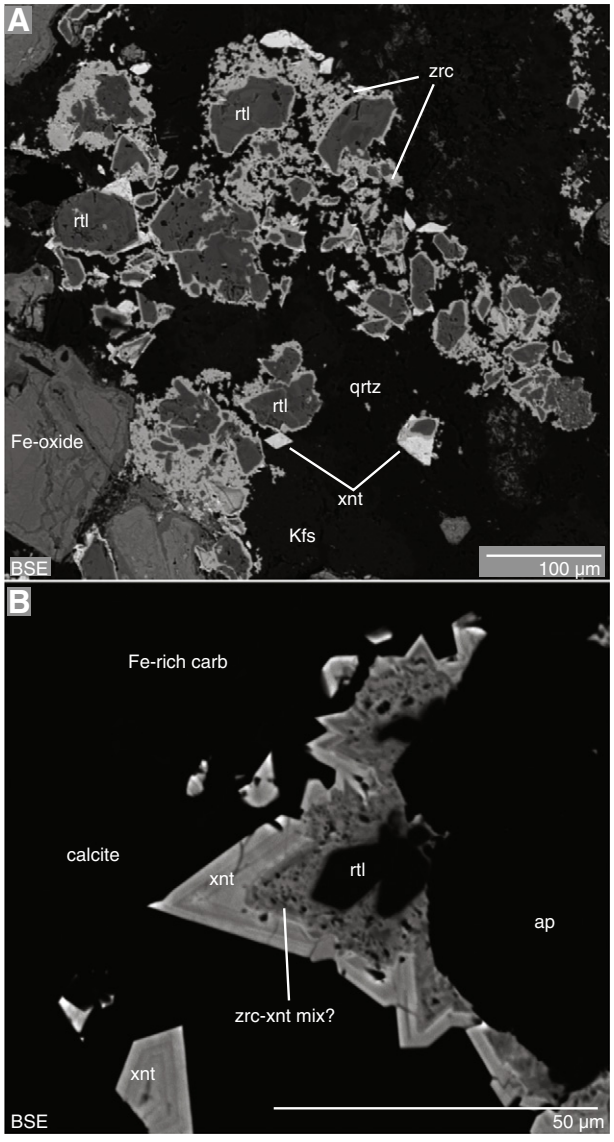


**Fig. 11.** BSE images of xenotime from Chenga Hill apatite-fluorite vein samples T0178B and T0178C. Xenotime mineralisation is divided into two types: (A) associated with Fe-oxides, rutile and zircon; and (B) overgrowths on apatite in late calcite, with associated rutile and zircon. Abbreviations same as Fig. 2.

homogenisation temperature of the inclusions in fluorite, because of its crystallisation after the final apatite stages, provides an absolute minimum temperature for HREE mineralisation of approximately 160 °C.

### 5.3. Cause of HREE enrichment in apatite

Cross-cutting relationships and the fine-grained, stringer-like apatite texture indicates that apatite precipitated out of solution very early during the hydrothermal fluid evolution. Early precipitation of phosphate is logical as REE-phosphates are relatively insoluble in hydrothermal fluids, especially at elevated temperatures (Poitrasson et al., 2004; Cetiner et al., 2005; Gysi et al., 2015; Louvel et al., 2015; Zhou et al., 2016). The solubility of apatite in a hydrothermal fluid is less well constrained, but experiments in silicate melts show that it is more soluble than monazite and solubility increases with increasing NaCl concentration (Ayers and Watson, 1991; Wolf and London, 1995; Piccoli and Candela, 2002). The low solubility of apatite is also indicated by alteration assemblages of monazite, apatite and bastnäsite from Bayan Obo (Smith et al., 1999). It is unclear why apatite forms at Songwe, rather than monazite, especially given its lower solubility and the abundance of LREE. One possibility is that in alkali, $Cl^-$- or $F^-$-bearing fluids, monazite solubility could be greater than apatite, and in these situations, apatite has a greater capacity to incorporate high concentrations (up to 23 wt%) of the REE (Krenn et al., 2012). Alternatively, the abundance of Ca, from magmatic calcite, may have played a role, as apatite can readily be synthesised through reaction of P-bearing fluids with carbonates (Kasioptas et al., 2008, 2011).

The highly variable REE concentration in Ap-3 and Ap-4, indicates the hydrothermal fluid, or fluids, were capable of both transporting and fractionating the REE. One mechanism for fractionating the REE in a hydrothermal fluid could be though preferential stability of different REE complexes in solution. Fluoride, chloride and carbonate/bicarbonate complexes are viable candidates for REE transport and fractionation at Songwe. LREE-fluoride and -chloride complexes are more stable than their HREE equivalents in hydrothermal systems and could, therefore, fractionate the REE during transport between 150–400 °C (Migdisov et al., 2009; Williams-Jones et al., 2012). Similar fractionation mechanisms have been proposed at the Nechalacho deposit, Canada, Pivot Creek, New Zealand and in late-stage apatite at Tundulu (Sheard et al., 2012; Williams-Jones et al., 2012; Cooper et al., 2015; Broom-Fendley et al., 2016a). Some depositional models for the REE in alkaline systems consider sulphate as an important ligand for REE transport (e.g. Xie et al., 2009, 2015). However, our new fluid inclusion and mineralogical data indicates this is not likely to be a major fluid component. Furthermore, experimentally derived stability constants for LREE and HREE sulphate complexes are similar and would therefore be unlikely to cause

**Table 5**
Average xenotime compositions (sample T0178).

| Concentration (wt%) | Overgrowths on apatite | | Associated with rutile, zircon and Fe-oxides | |
|---|---|---|---|---|
| | Avg. ($n = 16$) | 2SD | Avg. ($n = 9$) | 2SD |
| $SiO_2$ | 0.82 | 0.89 | 0.58 | 0.84 |
| $P_2O_5$ | 32.86 | 2.99 | 33.89 | 2.91 |
| CaO | 0.51 | 0.81 | 0.30 | 0.56 |
| FeO | 0.47 | 2.05 | 0.58 | 2.52 |
| $Y_2O_3$ | 47.95 | 3.77 | 48.48 | 4.66 |
| $Nd_2O_3$ | 0.06 | 0.07 | 0.08 | 0.06 |
| $Sm_2O_3$ | 0.13 | 0.17 | 0.14 | 0.24 |
| $Eu_2O_3$ | 0.11 | 0.14 | 0.14 | 0.16 |
| $Gd_2O_3$ | 0.98 | 0.76 | 1.17 | 1.39 |
| $Tb_2O_3$ | 0.34 | 0.25 | 0.35 | 0.33 |
| $Dy_2O_3$ | 5.12 | 1.20 | 5.43 | 2.59 |
| $Ho_2O_3$ | 1.41 | 0.27 | 1.44 | 0.30 |
| $Er_2O_3$ | 3.80 | 0.54 | 3.99 | 1.10 |
| $Tm_2O_3$ | 0.49 | 0.16 | 0.55 | 0.13 |
| $Yb_2O_3$ | 2.63 | 0.67 | 2.59 | 1.20 |
| $Lu_2O_3$ | 0.60 | 0.16 | 0.52 | 0.14 |
| $ThO_2$ | 2.00 | 1.65 | 0.56 | 0.79 |
| $UO_2$ | 0.25 | 0.33 | 0.13 | 0.15 |
| PbO | 0.38 | 0.07 | 0.37 | 0.04 |
| Total | 100.85 | 2.71 | 101.21 | 4.12 |
| *Formula calculated to 4 (O)* | | | | |
| Si | 0.028 | 0.031 | 0.019 | 0.029 |
| P | 0.935 | 0.045 | 0.951 | 0.045 |
| Ca | 0.019 | 0.030 | 0.011 | 0.020 |
| Fe | 0.013 | 0.059 | 0.016 | 0.073 |
| Y | 0.857 | 0.036 | 0.856 | 0.074 |
| Nd | 0.001 | 0.003 | 0.001 | 0.001 |
| Sm | 0.002 | 0.002 | 0.002 | 0.003 |
| Eu | 0.001 | 0.002 | 0.002 | 0.002 |
| Gd | 0.011 | 0.009 | 0.013 | 0.016 |
| Tb | 0.004 | 0.003 | 0.004 | 0.004 |
| Dy | 0.055 | 0.014 | 0.058 | 0.028 |
| Ho | 0.015 | 0.003 | 0.015 | 0.003 |
| Er | 0.040 | 0.005 | 0.042 | 0.011 |
| Tm | 0.005 | 0.002 | 0.006 | 0.001 |
| Yb | 0.027 | 0.007 | 0.026 | 0.012 |
| Lu | 0.006 | 0.002 | 0.005 | 0.001 |
| Th | 0.016 | 0.014 | 0.005 | 0.006 |
| U | 0.002 | 0.003 | 0.001 | 0.001 |
| Pb | 0.003 | 0.001 | 0.003 | 0.000 |
| Y-site | 1.078 | 0.060 | 1.064 | 0.060 |
| P-site | 0.963 | 0.029 | 0.971 | 0.020 |

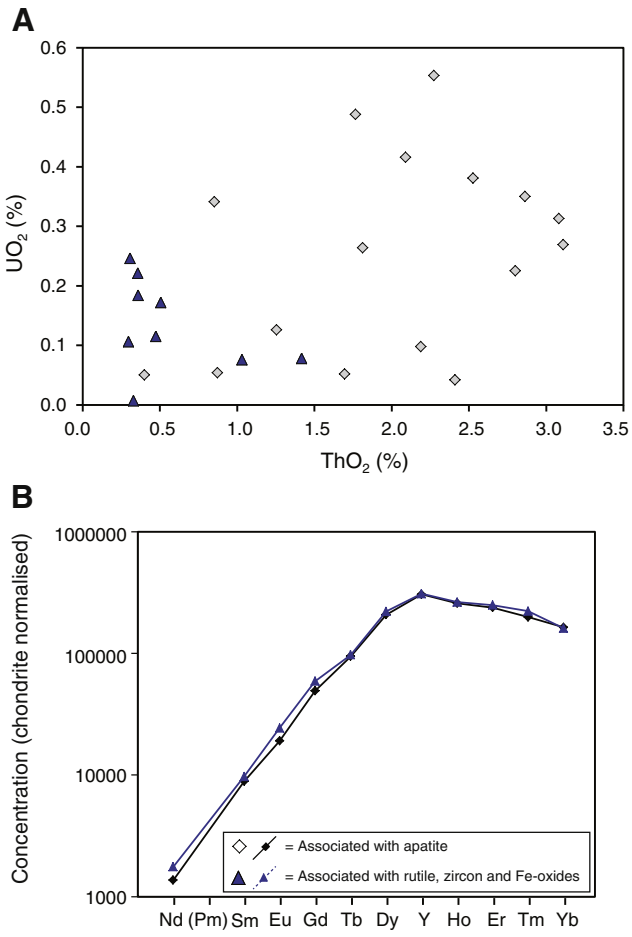


**Fig. 12.** Variation in U, Th and the REE between different xenotime types in apatite-fluorite veins. REE distributions normalised using values from McDonough and Sun (1995).

fractionation of the REE (Migdisov et al., 2006; Migdisov and Williams-Jones, 2008).

If the REE are complexed by fluoride or chloride, then rapid precipitation of apatite would lead to the destabilisation of REE complexes (Migdisov and Williams-Jones, 2014; Louvel et al. 2015). This is likely to occur through back-reaction of the exsolved fluid with the host carbonatite, though depressurisation/degassing or cooling could also lead to precipitation. Owing to their lower stability, the HREE complexes would preferentially destabilise over the LREE equivalents, leading to incorporation of the HREE into the precipitated apatite. LREE-complexes with $F^-$ or $Cl^-$ would remain in solution and subsequent evolution and cooling of the exsolved fluid could lead to the latter precipitation of LREE fluorocarbonates, strontianite and baryte. This implies that fluoride, sulphate and carbonate remain in solution after crystallisation of apatite.

It is difficult to envisage extensive transport of acidic REE-chloride and/or fluoride complexes in a carbonate-rich environment. Such fluids would rapidly react with the host carbonatite and precipitate. An alternative mechanism is carbonate complexation and transportation. $CO_2$ concentrations are high in carbonatitic fluids, and carbonate complexes could be a major carrier of the REE, especially given their 'hard' nature (Pearson, 1963). Limited experimental data on the differential stability of REE-carbonate complexes means that it is difficult to assess their importance in the fractionation of the REE at Songwe. It is postulated that REE-carbonate complexes could have different stabilities between the LREE and the HREE, in a manner akin to the stability of fluoride and chloride REE complexes (e.g. Williams-Jones et al., 2012).

If the REE are complexed by carbonate, then $CO_2$ degassing could be a viable depositional mechanism. The presence of mixed LV, LLV and V fluid inclusions in Ap-3 suggests that un-mixing and degassing is taking place. This would rapidly remove $CO_2$ from a fluid, potentially destabilising REE-carbonate complexes and leading to REE substitution in apatite. Such a depositional mechanism is also supported by the O isotope composition of the apatite at Songwe Hill, which ranges between −1 to +3‰ (VSMOW). These values, which are more negative than the primary igneous carbonatite field, correspond with the modelled composition of apatite crystallising from a cooling $CO_2$-rich fluid (Broom-Fendley et al., 2016b).

### 5.4. Further hydrothermal alteration

The presence of extensive HREE-rich fluorite mineralisation associated with Ap-4 and xenotime, late in the paragenesis, indicates that some remobilisation of the HREE took place. Fluid inclusions from fluorite show that this occurred at about 160 °C, comparable with mineralisation from many other carbonatite-related fluorite deposits (Palmer and Williams-Jones, 1996; Williams-Jones and Palmer, 2002; Bühn et al., 2002). It is unlikely that rapid precipitation of apatite caused this late mineralisation stage, and therefore an alternative solution is required. One such possibility is that the late, low T, fluorite mineralising fluids caused reprecipitation of apatite, facilitated by the retrograde

**Table 6**
Trace element concentrations (ppm) of fluorite from LA ICP-MS (sample U4909).

| Spot | F1 | F2 | F3 | F4 | F5 | F6 | F7 | F9 | F10 | F14 | F15 | F16 | F17 | F18 | F19 | F20 |
|---|---|---|---|---|---|---|---|---|---|---|---|---|---|---|---|---|
| Na | 52 | 150 | 190 | 68 | 130 | 240 | 62 | 170 | 74 | 41 | 39 | 110 | 120 | 67 | 98 | 80 |
| Mg | 8.0 | 9.3 | 8.2 | 39 | 8.7 | 8.9 | 180 | 36 | 7.3 | 7.4 | 660 | 8.0 | 32 | 28 | 170 | 62 |
| Al | 5.6 | 19 | 11.1 | 11 | 23 | 39 | 280 | 8.9 | 9.9 | 8.9 | 5.8 | 12 | 45 | 120 | 150 | 30 |
| K | 2.5 | 7.2 | 9.8 | 3.2 | 5.7 | 10 | 23 | 2.9 | 2.2 | 3.5 | 6.0 | 4.9 | 9.8 | 17 | 20 | 4.4 |
| Mn | 2.9 | 1.7 | 1.4 | 0.87 | 1.6 | 3.5 | 1.1 | 3.1 | 0.79 | 0.36 | 1.9 | 22 | 22 | 13 | 120 | 27 |
| Fe | 31 | 3.7 | 11 | 3.8 | 3.5 | 9.1 | 35 | 9.3 | 1.3 | 5.3 | 9.8 | 19 | 45 | 80 | 100 | 61 |
| Co | 1.7 | 0.06 | 0.48 | 0.12 | 0.19 | 0.25 | 0.53 | 0.06 | 0.28 | 0.04 | 0.70 | 0.14 | 0.06 | 0.80 | 0.77 | 1.3 |
| Rb | – | 0.12 | 0.09 | – | 0.07 | 0.10 | 0.14 | 0.13 | 0.15 | 0.09 | 0.02 | 0.27 | 0.32 | 0.28 | 0.36 | 0.15 |
| Sr | 1400 | 1400 | 1800 | 1800 | 1100 | 1200 | 1400 | 940 | 1900 | 1100 | 900 | 1100 | 800 | 880 | 1200 | 1100 |
| Y | 410 | 530 | 770 | 770 | 760 | 690 | 480 | 580 | 810 | 530 | 340 | 860 | 880 | 480 | 1100 | 720 |
| Ba | 1.4 | 28 | 4.3 | 8.6 | 11 | 14 | 2.7 | 2.8 | 7.4 | 1.3 | 2.6 | 7.5 | 3.4 | 1.7 | 2.1 | 7.9 |
| La | 3.6 | 8.5 | 4.7 | 9.1 | 4.0 | 7.8 | 1.1 | 5.7 | 20 | 0.74 | 2.5 | 100 | 5.4 | 3.1 | 2.7 | 19 |
| Ce | 5.5 | 22 | 7.8 | 16 | 7.2 | 15 | 1.7 | 9.4 | 30 | 1.9 | 2.1 | 150 | 11 | 7.0 | 4.9 | 37 |
| Pr | 0.43 | 2.3 | 0.90 | 1.9 | 0.87 | 1.2 | 0.19 | 0.99 | 2.5 | 0.16 | 0.26 | 13 | 1.4 | 0.88 | 0.55 | 2.8 |
| Nd | 1.9 | 8.4 | 4.2 | 8.1 | 4.3 | 5.2 | 1.2 | 6.0 | 10 | 1.1 | 1.3 | 58 | 5.9 | 4.9 | 2.5 | 7.9 |
| Sm | 0.34 | 2.5 | 0.90 | 2.5 | 1.4 | 1.6 | 0.57 | 3.3 | 2.9 | 1.0 | 0.62 | 11 | 2.1 | 1.9 | 1.5 | 1.8 |
| Eu | 0.24 | 1.4 | 0.80 | 1.7 | 1.1 | 1.1 | 0.55 | 3.0 | 1.9 | 1.2 | 0.59 | 5.6 | 1.89 | 1.25 | 1.29 | 1.43 |
| Gd | 2.0 | 6.7 | 5.2 | 11 | 7.4 | 6.6 | 3.6 | 20 | 13 | 8.0 | 3.6 | 21 | 13 | 8.3 | 10 | 6.8 |
| Tb | 0.85 | 3.3 | 2.2 | 4.7 | 3.1 | 2.7 | 1.3 | 10 | 5.1 | 2.4 | 1.4 | 6.0 | 6.6 | 2.6 | 5.8 | 3.4 |
| Dy | 8.5 | 32 | 23 | 50 | 30 | 25 | 13 | 85 | 54 | 19 | 15 | 50 | 67 | 27 | 66 | 27 |
| Ho | 2.9 | 8.3 | 8.2 | 12 | 9.5 | 7.9 | 3.5 | 24 | 15 | 6.1 | 3.9 | 14 | 19 | 7.7 | 18 | 9.1 |
| Er | 9.3 | 30 | 28 | 41 | 27 | 23 | 12 | 58 | 52 | 18 | 11 | 45 | 59 | 22 | 54 | 31 |
| Tm | 1.7 | 4.2 | 4.7 | 6.4 | 3.8 | 3.1 | 1.4 | 8.0 | 8.7 | 1.7 | 1.9 | 5.4 | 7.6 | 3.0 | 7.5 | 3.9 |
| Yb | 14 | 34 | 29 | 47 | 27 | 26 | 10 | 55 | 73 | 9.9 | 14 | 40 | 48 | 20 | 50 | 39 |
| Lu | 1.9 | 5.1 | 4.6 | 7.0 | 3.8 | 3.5 | 1.6 | 6.3 | 12 | 1.9 | 1.6 | 6.5 | 5.7 | 3.1 | 6.1 | 4.6 |
| Pb | 0.04 | 0.61 | 0.10 | 0.07 | 0.10 | 0.12 | 0.22 | 0.45 | 0.06 | 0.08 | 0.16 | 0.44 | 1.4 | 0.46 | 4.65 | 3.6 |
| Th | 0.35 | 54 | 1.6 | 2.8 | 4.6 | 3.7 | 2.9 | 14 | 4.0 | 2.6 | 1.1 | 33 | 4.6 | 2.6 | 3.1 | 13 |
| U | 0.08 | 0.27 | 0.08 | 0.03 | 0.16 | 0.13 | 0.08 | 0.06 | 0.02 | 0.18 | 0.06 | 0.36 | 0.35 | 0.22 | 0.24 | 0.32 |

Note, — denotes elements below detection.

solubility of REE-phosphates (Poitrasson et al., 2004; Cetiner et al., 2005; Gysi et al., 2015; Louvel et al., 2015). Fluorine and/or chlorine, from the fluorite-mineralising fluid, attacked earlier REE-bearing apatite, preferentially removing the HREE and Y. Subsequently, this fluid re-precipitated Ap-4 and xenotime as a later, more HREE-rich, generation.

### 5.5. Source of the HREE-rich fluids

A hydrothermal model is favoured to explain the REE mineralisation at Songwe, and the prevalence of HREE-enriched apatite over typical ovoid apatite from carbonatites. The reasons for the extensive development of this hydrothermal fluorapatite at Songwe but not at other carbonatites in the Chilwa Alkaline Province are important to understand.

The source for the hydrothermal fluid assumed in this depositional model is exsolution from the carbonatite during its evolution. Fluid exsolution during carbonatite ascent, decompression and cooling is a process that occurs in many carbonatites, and is commonly responsible for LREE, fluorite and baryte mineralisation (Le Bas, 1989; Rankin, 2005). The composition of the exsolved fluids is poorly understood but, from the limited studies where they have been characterised, they are generally considered to be composed of Na-K-chloride-carbonate/bicarbonate brines (Rankin, 2005). The only study where the chemistry of these fluids has been characterised shows that they can be rich in the REE (up to 40,000 ppm total REE) as well as Ba, Sr, Na and K (Bühn and Rankin, 1999).

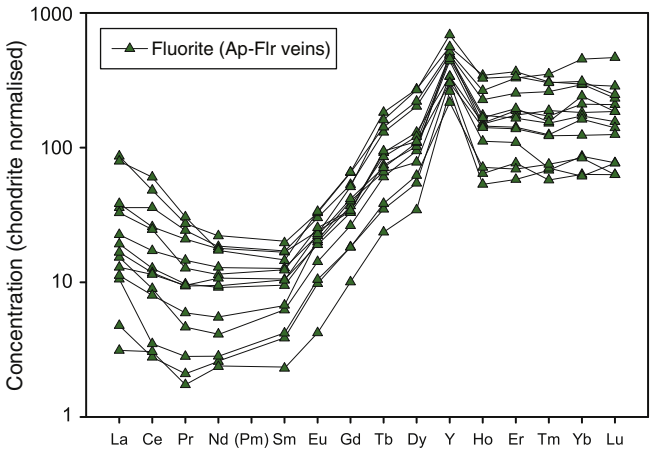


**Fig. 13.** Chondrite-normalised REE distribution of fluorite from apatite-fluorite veins. Chondrite values from McDonough and Sun (1995).

An alternative, more speculative, possibility is that the fluid source was the neighbouring Mauze nepheline syenite intrusion rather than the Songwe carbonatite itself (Fig. 1). Mauze has been dated as, within uncertainty, the same age as Songwe Hill (Broom-Fendley, 2015), and therefore would have been crystallising and cooling when Songwe was emplaced. It is possible that acidic, REE-bearing, fluids were exsolved during the late stage evolution of Mauze. Analyses of potentially-similar fluids from the Capitan Pluton, New Mexico, indicate that such fluids have the capacity to transport relatively high concentrations of the REE (200–1300 ppm), although this is commonly LREE-dominant (Banks et al., 1994). Such fluids could be exsolved from Mauze and react with the carbonate at Songwe to form apatite, akin to skarn reactions (cf. Estrade et al., 2015). Whole-rock, MREE-depleted REE distributions of samples from Mauze and low REE and $P_2O_5$ concentrations support this hypothesis, potentially indicating removal of the MREE (Broom-Fendley, 2015). However, the low Mn and high Sr concentrations of the late apatite are strong evidence for a carbonatitic origin and this hypothesis is therefore unlikely.

A third possibility is that mineralisation was caused by mixing of carbonatite-derived fluids with meteoric water, driven by the cooling of Songwe and/or Mauze. Mauze is a more likely candidate for this 'heat-engine' owing to its much larger size. Evidence for hydrothermal activity associated with syenite-granite at Zomba, in the north of the Chilwa Alkaline Province, lends support to this notion. Here, hydrothermal fluids with temperatures, calculated by Ti in zircon thermometry, of approximately 500–600 °C occurred for up to 3 Ma after emplacement (Soman et al., 2010). Furthermore, for the same intrusion, Eby et al.

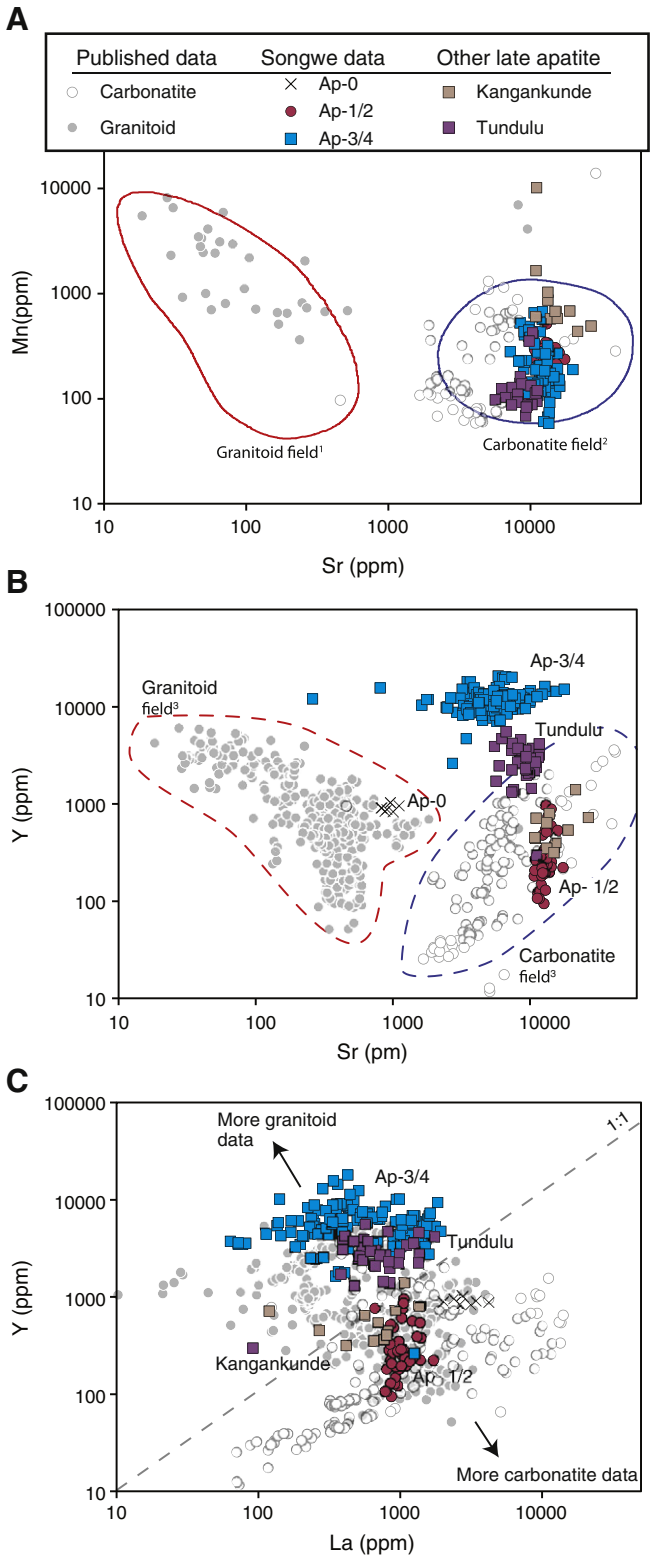


**Fig. 14.** Comparison of REE concentrations with published carbonatite and granitoid apatite compositions (see Supplementary information for data sources) and late-stage apatite from other Malawian carbonatites (Broom-Fendley et al. 2016a). [1]Apatite classification fields after Belousova et al. (2002); [2]Combined fields from Belousova et al. (2002) and Hogarth (1989); [3]Fields after Belousova et al. (2002) and Hogarth (1989), redrawn to better represent the wider compositional range when incorporating additional published data.

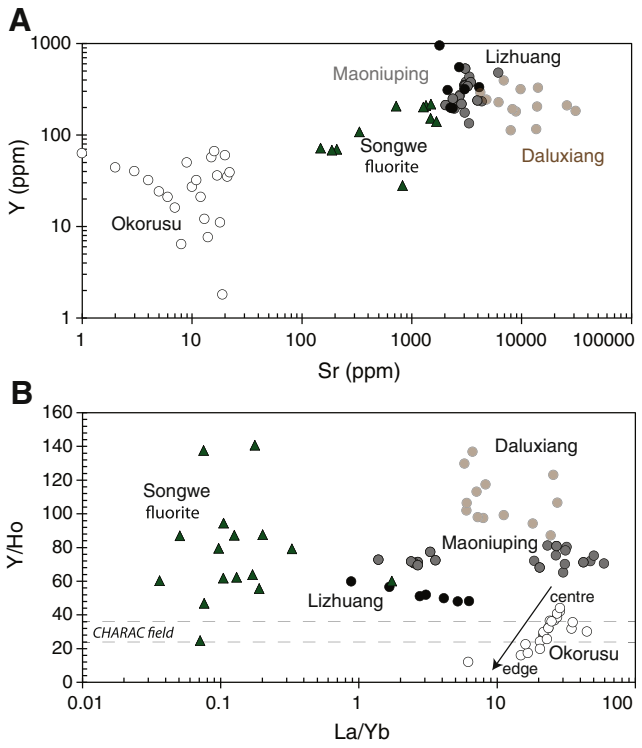


**Fig. 15.** Composition of Songwe fluorite compared to other carbonatite fluorite. Data sources: Okorusu, Bühn et al., 2003; Maoniuping, Daluxiang, Lizhuang, Xu et al., 2012. CHARAC field after Bau, 1996.

(1995) calculated, from K-Ar amphibole and fission-track zircon ages, that the cooling rate of Zomba was approximately 23 °C/Ma. None of the other carbonatites in the Chilwa Alkaline Province are associated with such large intrusions and the presence of the Mauze 'heat-engine' could be the important factor in differentiating the mineralisation at Songwe from the other carbonatites in the province.

## 6. Conclusions and implications

The principal REE-bearing minerals at the Songwe Hill carbonatite, Malawi, are synchysite-(Ce) and fluorapatite, together with minor xenotime-(Y), parisite-(Ce) and florencite-(Ce).

Comparison of apatite compositions at Songwe with other carbonatite- and granitoid-hosted apatite indicates that apatite from Songwe is the most HREE-rich apatite yet documented. This apatite composition gives the Songwe Hill REE deposit a higher proportion of HREE than almost all other carbonatite-related REE deposits. Such ore deposits, with significant amounts of HREE, are particularly sought after.

Five different apatite groups have been identified at Songwe (Ap-0–Ap-4). Ap-0 occurs in fenite only. Ap-1 crystallised in early calcite carbonatite and is LREE-enriched. Progressive levels of HREE enrichment then occur in Ap-2, -3 and -4 in later carbonatite generations. The main HREE-enriched and most abundant apatite, Ap-3, crystallised in a (carbo)-hydrothermal environment that produced a Y/Ho anomaly, fluid inclusions and formed veins and stringers cutting earlier carbonatite. The precipitation of Ap-3 preceded crystallisation of synchysite-(Ce), the main LREE mineral, as indicated by the termination of Ap-3 veins by an assemblage of, synchysite-(Ce), strontianite, baryte and calcite.

The transport and fractionation of the REE observed at Songwe partly supports the hypothesis of Migdisov and Williams-Jones (2014) and Williams-Jones et al. (2012) regarding preferential LREE solubility as chloride complexes in which the HREE are precipitated first and LREE

are retained in solution. Although the results for HREE-enriched Ap-3 and later synchysite-(Ce) are consistent with this hypothesis, there is also evidence that fluoride and carbonate complexation may have had a substantial role.

A carbonatite-derived fluid source is favoured; where hydrothermal fluids were exsolved as the carbonatite melt ascended, decompressed and cooled. A possible explanation for the presence of large amounts of fluorapatite at Songwe Hill but not at other Chilwa carbonatite complexes is the presence of the nearby larger Mauze nepheline syenite intrusion, which could have acted as a heat engine to drive a hydrothermal circulation system. The other Chilwa carbonatites do not have these kind of associated larger nepheline syenite intrusions.

These results should be applicable to help exploration models for other carbonatite complexes. Anhedral, late apatite and mineral assemblages at the margins of the complex are preferential targets for higher proportions of HREE.

## Acknowledgements

Thanks are due to A. Kearsley, J. Spratt (NHM), B. Perkins (Aberystwyth), S. Chenery and L. Field (BGS) for analytical assistance. A.E. Williams-Jones (McGill) and J. Naden (BGS) helped with fluid inclusion analyses. The comments Elisa Barbosa and an anonymous reviewer significantly improved this manuscript. This study was funded by a NERC BGS studentship to SBF (NEE/J50318/1; S208), the SoS RARE consortium (NE/M011429/1) and Mkango Resources Ltd. SBF is also grateful to the SEG and the Geological Society for travel grants associated with this project. AGG publishes with the permission of the Executive Director of the BGS.

## Appendix A. Supplementary data

Supplementary data to this article can be found online at http://dx.doi.org/10.1016/j.oregeorev.2016.10.019.

## References

Andersen, A.K., Clark, J.G., Larson, P.B., Neill, O.K., 2016. Mineral chemistry and petrogenesis of a HFSE(+HREE) occurrence, peripheral to carbonatites of the Bear Lodge alkaline complex, Wyoming. Am. Min. 101, 1604–1623.

Andrade, F., Möller, P., Lüders, V., Dulski, P., Gilg, H., 1999. Hydrothermal rare earth elements mineralization in the Barra do Itapirapuã carbonatite, southern Brazil: behaviour of selected trace elements and stable isotopes (C, O). Chem. Geol. 155, 91–113.

Ayers, J.C., Watson, E.B., 1991. Solubility of apatite, monazite, zircon, and rutile in supercritical aqueous fluids with implications for subduction zone geochemistry. Philos. Trans. R. Soc. Lond. A Phys. Eng. Sci. 335, 365–375.

Banks, D.A., Yardley, B.W.D., Campbell, A.R., Jarvis, K.E., 1994. REE composition of an aqueous magmatic fluid: a fluid inclusion study from the Capitan Pluton, New Mexico, U.S.A. Chem. Geol. 113, 259–272.

Bau, M., 1996. Controls on the fractionation of isovalent trace elements in magmatic and aqueous systems: evidence from Y/Ho, Zr/Hf, and lanthanide tetrad effect. Contrib. Miner. Petr. 123, 323–333.

Belousova, E., Griffin, W., O'Reilly, S.Y., Fisher, N., 2002. Apatite as an indicator mineral for mineral exploration: trace-element compositions and their relationship to host rock type. J. Geochem. Explor. 76, 45–69.

Bodnar, R., 1993. Revised equation and table for determining the freezing point depression of $H_2O$–NaCl solutions. Geochim. Cosmochim. Acta 57, 683–684.

Bodnar, R., 2003. Introduction to fluid inclusions. In: Samson, I., Anderson, A., Marshall, D. (Eds.), Fluid Inclusions: Analysis and Interpretation. Mineral. Assoc. Canada 32, pp. 1–8 Short Course.

Bühn, B., Rankin, A., 1999. Composition of natural, volatile-rich Na–Ca–REE-Sr carbonatitic fluids trapped in fluid inclusions. Geochim. Cosmochim. Acta 63, 3781–3797.

Bühn, B., Wall, F., Le Bas, M., 2001. Rare-earth element systematics of carbonatitic fluorapatites, and their significance for carbonatite magma evolution. Contrib. Miner. Petr. 141, 572–591.

Bühn, B., Rankin, A., Schneider, J., Dulski, P., 2002. The nature of orthomagmatic, carbonatitic fluids precipitating REE, Sr-rich fluorite: fluid inclusion evidence from the Okorusu fluorite deposit, Namibia. Chem. Geol. 186, 75–98.

Bühn, B., Schneider, J., Dulski, P., Rankin, A., 2003. Fluid–rock interaction during progressive migration of carbonatitic fluids, derived from small-scale trace element and Sr, Pb isotope distribution in hydrothermal fluorite. Geochim. Cosmochim. Acta 67, 4577–4595.

Broom-Fendley, S., 2015. Targeting Heavy Rare Earth Elements in Carbonatite Complexes. PhD thesis. University of Exeter.

Broom-Fendley, S., Styles, M.T., Appleton, J.D., Gunn, G., Wall, F., 2016a. Evidence for dissolution-reprecipitation of apatite and preferential LREE mobility in carbonatite-derived late-stage hydrothermal processes. Am. Min. 101, 596–611.

Broom-Fendley, S., Heaton, T., Wall, F., Gunn, G., 2016b. Tracing the fluid source of heavy REE mineralisation in carbonatites using a novel method of oxygen-isotope analysis in apatite: the example of Songwe Hill, Malawi. Chem. Geol. 440, 275–287.

Campbell, L.S., Henderson, P., 1997. Apatite paragenesis in the Bayan Obo REE-Nb-Fe ore deposit, inner Mongolia, China. Lithos 42, 89–103.

Cetiner, Z.S., Wood, S.A., Gammons, C.H., 2005. The aqueous geochemistry of the rare earth elements. Part XIV. The solubility of rare earth element phosphates from 23 to 150 °C. Chem. Geol. 217, 147–169.

Chakhmouradian, A., Wall, F., 2012. Rare earth elements: minerals, mines, magnets (and more). Elements 8, 333–340.

Cooper, A.F., Collins, A.K., Palin, J.M., Spratt, J., 2015. Mineralogical evolution and REE mobility during crystallisation of ancylite-bearing ferrocarbonatite, Haast River, New Zealand. Lithos 216–217, 324–337.

Croll, R., Swinden, S., Hall, M., Brown, C., Beer, G., Scheepers, J., Redellinghuys, T., Wild, G., Trusler, G., 2014. Mkango Resources Limited, Songwe REE Project, Malawi: NI 43-101 Pre-feasibility Report. Technical Report. MSA Group (Pty) Ltd.

Diamond, L.W., 1992. Stability of $CO_2$ clathrate hydrate + $CO_2$ liquid + $CO_2$ vapour + aqueous KCl-NaCl solutions: experimental determination and application to salinity estimates of fluid inclusions. Geochim Cosmochim Acta 56, 273–280.

Doroshkevich, A.G., Viladkar, S.G., Ripp, G.S., Burtseva, M.V., 2009. Hydrothermal REE mineralization in the Amba Dongar carbonatite complex, Gujarat, India. Can. Mineral. 47, 1105–1116.

Eby, G.N., 1975. Abundance and distribution of the rare-earth elements and yttrium in the rocks and minerals of the Oka carbonatite complex, Quebec. Geochim. Cosmochim. Acta 39, 597–620.

Eby, G.N., Roden-Tice, M., Krueger, H., Ewing, W., Faxon, E., Woolley, A., 1995. Geochronology and cooling history of the northern part of the Chilwa Alkaline Province, Malawi. J. Afr. Earth Sci. 20, 275–288.

Estrade, G., Salvi, S., Béziat, D., Williams-Jones, A.E., 2015. The origin of skarn-hosted rare-metal mineralization in the Ambohimirahavavy Alkaline Complex, Madagascar. Econ. Geol. 110, 1485–1513.

European Commission, 2014. Report on Critical Raw Materials for the EU, Report of the Ad Hoc Working Group on Defining Critical Raw Materials.Technical report. Available at. http://ec.europa.eu/DocsRoom/documents/10010/attachments/1/translations/en/renditions/native (Archived by WebCite® at http://www.webcitation.org/6cJu6Nnpj).

Fleischer, M., Altschuler, Z., 1986. The lanthanides and yttrium in minerals of the apatite group — an analysis of the available data. Neues Jahrbuch fuer Mineralogie, Monatshefte 10, 467–480.

Förster, H.-J., 1998. The chemical composition of REE-Y-Th-U-rich accessory minerals in peraluminous granites of the Erzgebirge-Fichtelgebirge region, Germany; part II, xenotime. Am. Min. 83, 1302–1315.

Gagnon, J.E., Samson, I.M., Fryer, B.J., Williams-Jones, A.E., 2003. Compositional heterogeneity in fluorite and the genesis of fluorite deposits: insights from LA–ICP–MS analysis. Can. Mineral. 41, 365–382.

Garson, M., 1965. Carbonatites in southern Malawi. Bull. Geol. Surv. Malawi 15.

Gunn, A.G. (Ed.), 2014. Critical Metals Handbook. Wiley, New York.

Gysi, A.P., Williams-Jones, A.E., Harlov, D., 2015. The solubility of xenotime-(Y) and other HREE phosphates ($DyPO_4$, $ErPO_4$ and $YbPO_4$) in aqueous solutions from 100 to 250 °C and psat. Chem. Geol. 401, 83–95.

Hogarth, D., 1989. Pyrochlore, apatite and amphibole: distinctive minerals in carbonatite. In: Bell, K. (Ed.), Carbonatites: Genesis and Evolution. Unwin Hyman, London, pp. 105–148.

Hornig-Kjarsgaard, I., 1998. Rare earth elements in sövitic carbonatites and their mineral phases. J. Petrol. 39, 2105–2121.

Hughes, J.M., Rakovan, J.F., 2015. Structurally robust, chemically diverse: apatite and apatite supergroup minerals. Elements 11, 165–170.

Ihlen, P.M., Schiellerup, H., Gautneb, H., Skår, Ø., 2014. Characterization of apatite resources in Norway and their REE potential, a review. Ore Geol. Rev. 58, 126–147.

Kamenetsky, V.S., Mitchell, R.H., Maas, R., Giuliani, A., Gaboury, D., Zhitova, L., 2015. Chlorine in mantle-derived carbonatite melts revealed by halite in the St.-Honoré intrusion (Québec, Canada). Geology 43, 687–690.

Kapustin, I., 1980. Mineralogy of Carbonatites. Amerind Publishing Co., New Delhi.

Kasioptas, A., Perdikouri, C., Putnis, C., Putnis, A., 2008. Pseudomorphic replacement of single calcium carbonate crystals by polycrystalline apatite. Mineral. Mag. 72, 77–80.

Kasioptas, A., Geisler, T., Perdikouri, C., Trepmann, C., Gussone, N., Putnis, A., 2011. Polycrystalline apatite synthesized by hydrothermal replacement of calcium carbonates. Geochim. Cosmochim. Acta 75, 3486–3500.

Krenn, E., Harlov, D.E., Finger, F., Wunder, B., 2012. LREE redistribution among fluorapatite, monazite, and allanite at high pressures and temperatures. Am. Min. 97, 1881–1890.

Kynicky, J., Smith, M.P., Xu, C., 2012. Diversity of rare earth deposits: the key example of China. Elements 8, 361–367.

Ladenburger, S., Marks, M.A.W., Upton, B., Hill, P., Wenzel, T., Markl, G., 2016. Compositional variation of apatite from rift-related alkaline igneous rocks of the Gardar Province, south Greenland. Am. Min. 101, 612–626.

Le Bas, M., 1989. Diversification of carbonatite. In: Bell, K. (Ed.), Carbonatites: Genesis and Evolution. Unwin Hyman, London, pp. 428–447.

Le Bas, M., Handley, C., 1979. Variation in apatite composition in ijolitic and carbonatitic igneous rocks. Nature 279, 54–56.

Le Maître, R.W., Streckeisen, A., Zanettin, B., Le Bas, M.J., Bonin, B., Bateman, P., Lameyre, J., Sabine, P.A., Schmid, R., Sørensen, H., Woolley, A.R., 2002. Igneous rocks: a classification and glossary of terms: recommendations of the International Union of Geological Sciences. Subcommission on the Systematics of Igneous Rocks. Cambridge University Press.

Loges, A., Migdisov, A.A., Wagner, T., Williams-Jones, A.E., Markl, G., 2013. An experimental study of the aqueous solubility and speciation of Y (III) fluoride at temperatures up to 250 °C. Geochim. Cosmochim. Acta 123, 403–415.

Louvel, M., Bordage, A., Testemale, D., Zhou, L., Mavrogenes, J., 2015. Hydrothermal controls on the genesis of REE deposits: insights from an in situ XAS study of Yb solubility and speciation in high temperature fluids (T < 400 °C). Chem. Geol. 417, 228–237.

Mariano, A.N., 1989. Nature of economic mineralization in carbonatites and related rocks. In: Bell, K. (Ed.), Carbonatites: Genesis and Evolution. Unwin Hyman, London, pp. 149–176.

Mariano, A.N., Mariano, A., 2012. Rare earth mining and exploration in North America. Elements 8, 369–376.

McDonough, W., Sun, S., 1995. The composition of the earth. Chem. Geol. 120, 223–253.

Migdisov, A.A., Williams-Jones, A., 2008. A spectrophotometric study of Nd (III), Sm (III) and Er (III) complexation in sulfate-bearing solutions at elevated temperatures. Geochim. Cosmochim. Acta 72, 5291–5303.

Migdisov, A.A., Williams-Jones, A., 2014. Hydrothermal transport and deposition of the rare earth elements by fluorine-bearing aqueous liquids. Mineral. Deposita 49, 987–997.

Migdisov, A.A., Reukov, V., Williams-Jones, A., 2006. A spectrophotometric study of neodymium (III) complexation in sulfate solutions at elevated temperatures. Geochim. Cosmochim. Acta 70, 983–992.

Migdisov, A.A., Williams-Jones, A., Wagner, T., 2009. An experimental study of the solubility and speciation of the rare earth elements (III) in fluoride-and chloride-bearing aqueous solutions at temperatures up to 300 °C. Geochim. Cosmochim. Acta 73, 7087–7109.

Mitchell, R.H., 2014. Cathodoluminescence of apatite. Mineral. Assoc. Canada, Short Course Ser. 45, 143–167.

Moore, M., Chakhmouradian, A.R., Mariano, A.N., Sidhu, R., 2015. Evolution of rare-earth mineralization in the Bear Lodge carbonatite, Wyoming: mineralogical and isotopic evidence. Ore Geol. Rev. 64, 499–521.

Ngwenya, B., 1994. Hydrothermal rare earth mineralisation in carbonatites of the Tundulu complex, Malawi: processes at the fluid/rock interface. Geochim. Cosmochim. Acta 58, 2061–2072.

Palmer, D., Williams-Jones, A., 1996. Genesis of the carbonatite-hosted fluorite deposit at Amba Dongar, India: evidence from fluid inclusions, stable isotopes, and whole rock-mineral geochemistry. Econ. Geol. 91, 934–950.

Pan, Y., Fleet, M.E., 2002. Compositions of the apatite-group minerals: substitution mechanisms and controlling factors. Rev. Mineral. Geochem. 48, 13–49.

Pearson, R.G., 1963. Hard and soft acids and bases. J. Am. Chem. Soc. 85, 3533–3539.

Poitrasson, F., Oelkers, E., Schott, J., Montel, J.-M., 2004. Experimental determination of synthetic $NdPO_4$ monazite end-member solubility in water from 21 °C to 300 °C: implications for rare earth element mobility in crustal fluids. Geochim. Cosmochim. Acta 68, 2207–2221.

Potter, E.G., Mitchell, R.H., 2005. Mineralogy of the deadhorse creek volcaniclastic breccia complex, northwestern Ontario, Canada. Contrib. Mineral. Petr. 150, 212–229.

Piccoli, P.M., Candela, P.A., 2002. Apatite in igneous systems. Rev. Mineral. Geochem. 48, 255–292.

Rankin, A., 2005. Carbonatite-associated rare metal deposits: composition and evolution of ore-forming fluids—the fluid inclusion evidence. Geol. Assoc. Canada, Short Course Notes 17, 299–314.

Schwinn, G., Markl, G., 2005. REE systematics in hydrothermal fluorite. Chem. Geol. 216, 225–248.

Sheard, E., Williams-Jones, A., Heiligmann, M., Pederson, C., Trueman, D., 2012. Controls on the concentration of zirconium, niobium, and the rare earth elements in the Thor Lake rare metal deposit, northwest territories, Canada. Econ. Geol. 107, 81–104.

Shepherd, T.J., Rankin, A.H., Alderton, D., 1985. A Practical Guide to Fluid Inclusion Studies. 239 pp. Blackie, Glasgow.

Simonetti, A., Bell, K., 1995. Nd, Pb, and Sr isotope systematics of fluorite at the Amba Dongar carbonatite complex, India; evidence for hydrothermal and crustal fluid mixing. Econ. Geol. 90, 2018–2027.

Smith, M., Henderson, P., Peishan, Z., 1999. Reaction relationships in the Bayan Obo Fe-REE-Nb deposit Inner Mongolia, China: implications for the relative stability of rare-earth element phosphates and fluorocarbonates. Contrib. Mineral. Petr. 134, 294–310.

Soman, A., Geisler, T., Tomaschek, F., Grange, M., Berndt, J., 2010. Alteration of crystalline zircon solid solutions: a case study on zircon from an alkaline pegmatite from Zomba–Malosa, Malawi. Contrib. Mineral. Petr. 160, 909–930.

Stoppa, F., Liu, Y., 1995. Chemical composition and petrogenetic implications of apatites from some ultra-alkaline Italian rocks. Eur. J. Mineral. 7, 391–402.

Ting, W., Burke, E.A., Rankin, A.H., Woolley, A.R., 1994. Characterisation and petrogenetic significance of $CO_2$, $H_2O$ and $CH_4$ fluid inclusions in apatite from the Sukulu carbonatite, Uganda. Eur. J. Mineral. 6, 787–803.

Verplanck, P.L., Mariano, A.N., Mariano, A., 2016. Rare earth element ore geology of carbonatites. Rev. Econ. Geol. 18, 5–32.

Wall, F., 2014. Rare Earth Elements. In: Gunn, A. (Ed.), Critical Metals Handbook. Wiley, New York.

Wall, F., Mariano, A., 1996. Rare earth minerals in carbonatites: a discussion centred on the Kangankunde Carbonatite, Malawi. In: Jones, A., Wall, F., Williams, C.T. (Eds.), Rare Earth Minerals: Chemistry Origin and Ore Deposits. Chapman and Hall, London, pp. 193–226.

Wall, F., Zaitsev, A., 2004. Rare earth minerals in Kola carbonatites. In: Wall, F., Zaitsev, A. (Eds.), Phoscorites and Carbonatites from Mantle to Mine: The Key Example of the Kola Alkaline Province. Mineralogical Society, London.

Wall, F., Niku-Paavola, V., Storey, C., Müller, A., Jeffries, T., 2008. Xenotime-(Y) from carbonatite dykes at Lofdal, Namibia: unusually low LREE:HREE ratio in carbonatite, and the first dating of xenotime overgrowths on zircon. Can. Mineral. 46, 861–877.

Walter, A.-V., Nahon, D., Flicoteaux, R., Girard, J., Melfi, A., 1995. Behaviour of major and trace elements and fractionation of REE under tropical weathering of a typical apatite-rich carbonatite from Brazil. Earth Planet Sci. Lett. 136, 591–602.

Walters, A., Goodenough, K., Hughes, H., Roberts, N., Gunn, A., Rushton, J., Lacinska, A., 2013. Enrichment of rare earth elements during magmatic and post-magmatic processes: a case study from the Loch Loyal syenite complex, northern Scotland. Contrib. Mineral. Petr. 166, 1177–1202.

Wang, L.-X., Marks, M.A., Wenzel, T., Von Der Handt, A., Keller, J., Teiber, H., Markl, G., 2014. Apatites from the Kaiserstuhl volcanic complex, Germany: new constraints on the relationship between carbonatite and associated silicate rocks. Eur. J. Mineral. 26, 397–414.

Williams, C.T., 1996. Analysis of rare earth minerals, pp. 327–348. A. Jones, F. Wall, and C. T. Williams (Eds.), Rare Earth Minerals: Chemistry Origin and Ore Deposits. Chapman and Hall, London, pp. 193–226.

Williams-Jones, A., Palmer, D., 2002. The evolution of aqueous–carbonic fluids in the Amba Dongar carbonatite, India: implications for fenitisation. Chem. Geol. 185, 283–301.

Williams-Jones, A., Migdisov, A., Samson, I., 2012. Hydrothermal mobilisation of the rare earth elements: a tale of "Ceria" and "Yttria". Elements 8, 355.

Wolf, M.B., London, D., 1995. Incongruent dissolution of REE-and Sr-rich apatite in peraluminous granitic liquids: differential apatite, monazite, and xenotime solubilities during anatexis. Am. Min. 80, 765–775.

Woolley, A., 2001. Alkaline Rocks and Carbonatites of the World. Part 3: Africa. The Geological Society, London.

Wyllie, P., Cox, K.G., Biggar, G.M., 1962. The habit of apatite in synthetic systems and igneous rocks. J. Petrol. 3, 238–243.

Xie, Y., Hou, Z., Yin, S., Dominy, S.C., Xu, J., Tian, S., Xu, W., 2009. Continuous carbonatitic melt–fluid evolution of a REE mineralization system: evidence from inclusions in the Maoniuping REE deposit, western Sichuan, China. Ore Geol. Rev. 36, 90–105.

Xie, Y., Li, Y., Hou, Z., Cook, D.R., Danyushevsky, L., Dominy, S.C., Yin, S., 2015. A model for carbonatite hosted REE mineralisation — the Mianning–Dechang REE belt, western Sichuan Province, China. Ore Geol. Rev. 70, 595–612.

Xu, C., Campbell, I.H., Allen, C.M., Huang, Z., Qi, L., Zhang, H., Zhang, G., 2007. Flat rare earth element patterns as an indicator of cumulate processes in the Lesser Qinling carbonatites, China. Lithos 95, 267–278.

Xu, C., Taylor, R.N., Li, W., Kynicky, J., Chakhmouradian, A.R., Song, W., 2012. Comparison of fluorite geochemistry from REE deposits in the Panxi region and Bayan Obo, China. J. Asian Earth Sci. 57, 76–89.

Zaitsev, A.N., Wall, F., Le Bas, M.J., 1998. REE-Sr-Ba minerals from the Khibina carbonatites, Kola Peninsula, Russia: their mineralogy, paragenesis and evolution. Mineral. Mag. 62, 225–250.

Zaitsev, A., Demény, A., Sindern, S., Wall, F., 2002. Burbankite group minerals and their alteration in rare earth carbonatites: source of elements and fluids (evidence from C–O and Sr–Nd isotopic data). Lithos 62, 15–33.

Zaitsev, A.N., Williams, C.T., Jeffries, T.E., Strekopytov, S., Moutte, J., Ivashchenkova, O.V., Spratt, J., Petrov, S.V., Wall, F., Seltmann, R., Borozdin, A.P., 2015. Rare earth elements in phoscorites and carbonatites of the Devonian Kola Alkaline Province, Russia: examples from Kovdor, Khibina, Vuoriyarvi and Turiy Mys complexes. Ore Geol. Rev. 64, 477–498.

Zhou, L., Mavrogenes, J., Spandler, C., Li, H., 2016. A synthetic fluid inclusion study of the solubility of monazite-(La) and xenotime-(Y) in H2O-Na-K-Cl-F-CO2 fluids at 800 °C and 0.5 GPa. Chem. Geol. 442, 121–129.

Zirner, A.L.K., Marks, M.A.W., Wenzel, T., Jacob, D.E., Markl, G., 2015. Rare earth elements in apatite as a monitor of magmatic andmetasomatic processes: the Ilímaussaq complex, South Greenland. Lithos 229, 12–22.